

UNIVERSITAT DE BARCELONA

FUNDAMENTAL PRINCIPLES OF DATA SCIENCE MASTER'S
THESIS

Characterization of Movement-related Neural States in NHP's

Author:
Michael DEPASS

Supervisor:
Dr. Ignasi Cos

*A thesis submitted in partial fulfillment of the requirements
for the degree of MSc in Fundamental Principles of Data Science*

in the

Facultat de Matemàtiques i Informàtica

September 1, 2020

UNIVERSITAT DE BARCELONA

Abstract

Facultat de Matemàtiques i Informàtica

MSc

Characterization of Movement-related Neural States in NHP's

by Michael DEPASS

The overall goal of the project was the principled characterization of neural states during movement execution before and after traumatic intervention (Muscimol inactivation or stroke). To this end we developed a machine learning pipeline to perform neural state classification using high dimensional EEG and LFP data. These neural data were collected while NHP's performed reward retrieval tasks involving reaching and grasping. An intervention was performed in the portion of the brain affecting movement of the right hand and the experiment was repeated. Three classification features were analyzed: spectral power, and functional connectivity which consisted of inter-signal covariance and correlation. These features were computed for nine frequency bands. Multinomial logistic regression (MLR) and 1-nearest neighbor (1-NN) classifiers were independently fit to each of the three types of classification features for all nine frequency bands (27 combinations). Classification performance was then analyzed in tasks of varying difficulty. MLR outperformed 1-NN and achieved AUC scores of above 0.8 for all tasks when fit to the highest frequency band power data. Lower frequency bands yielded considerably worse accuracies. Functional connectivity features yielded lower accuracies than spectral power features, though they far exceeded random chance. Finally, discriminative support networks were generated to further characterize the movement-related states.¹

¹Code available on [Github](#)

Acknowledgements

Firstly, I must thank my supervisor, Dr. Ignasi Cos, for his ever-present positive attitude and for providing me with guidance throughout the duration of the thesis project. He went above and beyond the call of duty by offering to process some of the data on both his work and personal computers. I am extremely grateful for his support. Secondly, I must acknowledge my wonderful parents, Linval and Jill, for instilling in me the logical and data-driven mindset that I am continuing to develop and refine today. I wouldn't be where I am today without them. Lastly, I feel obligated to thank a classmate of mine, Albert Garcia, for taking the time to break down complex topics that we covered throughout the master's degree program.

Chapter 1

Introduction

Local field potential data was collected by the Dancause Laboratory at the University of Montreal. We tested the hypothesis that we could differentiate neural states associated with specific movements before and after traumatic intervention (infarction). A secondary goal was to derive discriminative support networks in order to visualize the most significant inter and intra-region activity for each classification task. I will begin with a brief review of neural data and how machine learning has revolutionized Neuroscience. Subsequently I will discuss various foundational concepts for the current project such as the utility of high density multi-electrode arrays, functional connectivity, and spectral power. Finally I will provide a high-level summary of the project.

1.1 Neural Data

Neural data has been acquired for clinical and research purposes for over a century. In 1875 Richard Caton, a British physician, published findings regarding electrical activity recorded from the exposed cerebral hemispheres of monkeys and rabbits in the *British Medical Journal* (Caton and Schoenberg, 1974). This marked the beginning of what would become a full blown revolution in Neuroscience. Since then, a plethora of recording methodologies have been implemented, each with their own advantages and disadvantages. Two of the main criteria for comparing recording methodologies are spatial and temporal resolution. Figure ?? shows various neural data recording methodologies organized by their spatial and temporal resolution.

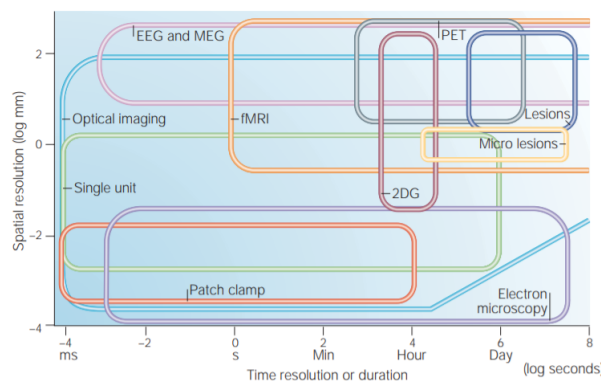


FIGURE 1.1 Neural recording methodologies organized by spatiotemporal resolution(Grinvald and Hildesheim, 2004)

The figure is by no means all-encompassing. In fact, new methodologies are being developed at an astonishing pace. Functional ultrasound (fUS), for example, is now being investigated as a possible alternative for whole brain imaging due to its impressive spatiotemporal resolution and sensitivity(Macé et al., 2018).

1.2 Electroencephalography and Local Field Potentials

For this thesis, electroencephalography (EEG) and local field potential (LFP) data were analyzed. EEG and LFP are both time series voltage data. In order to collect EEG and LFP data, electrodes are either surgically implanted or placed directly on the surface of the skin. The voltage between the electrodes and a reference is then recorded. In the case of EEG, the measured voltage is the aggregate of potentials generated by millions of neurons. LFP is much the same, however, it represents the aggregate of potentials across thousands of neurons rather than millions. A second key difference is that LFP always involves surgical implantation of electrodes and is often used to measure potentials at varying depths. Surgical implantation results in a better signal to noise ratio and less artifacts when compared to surface electrodes. This is a key advantage that this particular dataset provides over those analyzed in other similar work.

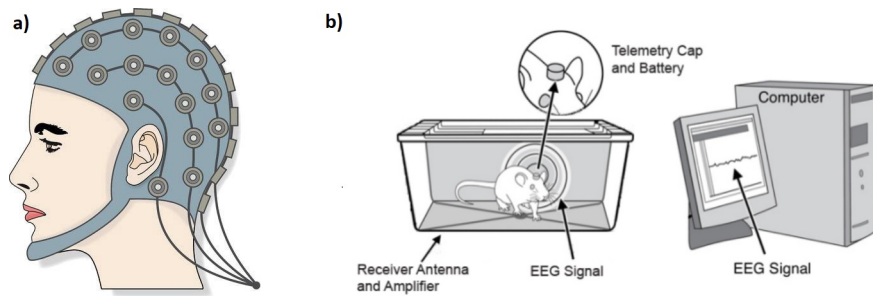


FIGURE 1.2 EEG modalities: a) Array of surface electrodes on human subject b) Intracranial electrodes implanted in mouse skull-cap. Wirelessly transmits signal to acquisition computer.

1.3 Neural Data Pre-processing

Neural recordings are necessarily encompassed by noise, from physiological and non-physiological sources alike. For example, it is exceedingly common, to see a spike in power at 50 Hz (and its harmonics) resulting from power supply noise contamination. For this reason, neural data is first passed through a pipeline of low and high pass filters to de-noise the signal as much as possible. Movement artifact is another common source of noise. Eye blinks, chewing, and facial expressions are known to produce electrical artifacts that are incorporated in the neural signals. This kind of noise cannot be filtered as it spans across frequencies and, thus, requires specific methods to remove it. One such method is independent component analysis — ICA (Lisha Sun, Ying Liu, and Beadle, 2005). ICA allows for the decomposition of signals into n statistically independent components.

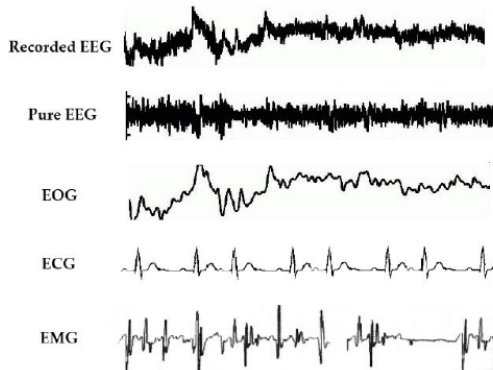


FIGURE 1.3 ICA components labeled according to their sources(Jiang, Bian, and Tian, 2019).

Once the signal has been decomposed, individual noisy and/or artefactual components may be identified (visually or by other machine learning methods), their contribution to the overall recording removed, and then the neural signal alone, ultimately recomposed. Filtering and ICA are just two of the most popular methods currently used for neural data pre-processing. Other common methods include wavelet transform, canonical correlation analysis, and empirical mode decomposition.

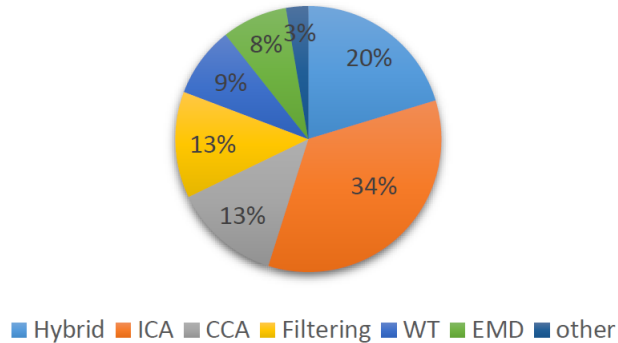


FIGURE 1.4 Prevalence of preprocessing techniques: percentage of number of references published over a three year period between 2016 and 2019(Jiang, Bian, and Tian, 2019).

1.4 Machine Learning in Neuroscience

Machine learning (ML) began seeing use in Neuroscience in the 1990's. Since then, its use has become increasingly widespread. According to Semantic Scholar, less than 1% of papers mentioning "Neuroscience" included the term "machine learning" in 1997. Now, however, roughly 80% of papers mentioning "Neuroscience" contain the term "machine learning" as well. There are several reasons for this radical increase, the first of which is the complexity, high-dimensionality, and noisiness of neural data. ML has been used to counteract these issues by performing dimensionality reduction and artifact detection. The second reason is the high prevalence of time consuming classification tasks traditionally performed manually by highly trained professionals. Sleep staging and brain lesion detection are two such tasks.

The two aforementioned reasons for the ML boom in Neuroscience involve taking advantage of ML to more efficiently learn about the brain, a third reason for the increase of ML in Neuroscience, however, is utilizing our understanding of neural processing to both improve upon and create new ML algorithms. In this thesis we will focus on the application of ML for artifact detection and classification of neural data.

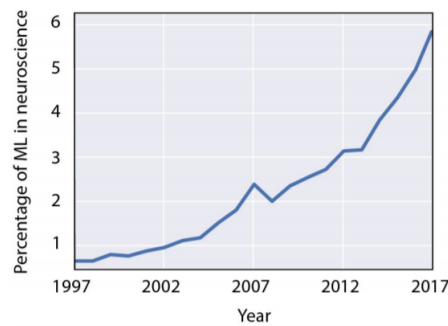


FIGURE 1.5 Prevalence of ML in Neuroscience over time(Glaser et al., 2018).

1.5 Neural Signal Classification

Classification of various neural data modalities has immensely impacted biology and medicine. MRI image data, for example, has been used to automatically classify brain tumors using powerful segmentation methods made possible by Convolutional Neural Networks (CNN). EEG and LFP data have also been used to perform various classification tasks. These tasks include emotion, mental workload, motor imagery, event related potentials, seizures, and sleep stage detection. A multitude of classifiers have been used to complete these tasks including: logistic regression, K-nearest neighbors, support vector machines, deep learning, tree-based methods, and many more.

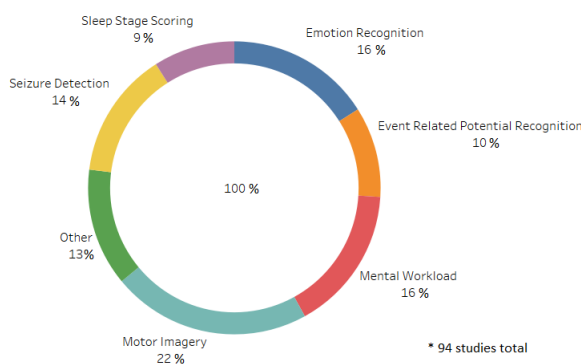


FIGURE 1.6 Breakdown of classification tasks utilizing EEG and deep learning(Craik, He, and Contreras-Vidal, 2019).

For this project, multinomial logistic regression (MLR) and K-nearest neighbors (KNN) were used. MLR is a popular classification due to it only making modest assumptions regarding the distribution of the data. KNN is non-parametric so it could outperform MLR if a non-linear solution is required. There is also a precedent for using these two methods for neural state classification and discriminative support network generation (Pallares et al., 2018). Using these methods allows us to directly compare performance.

1.5.1 Machine Learning Pipeline for EEG & LFP data

- The first step is to acquire and label the data, as with any supervised ML pipeline
- The signal must be split into training, validation, and test sets.
- The pre-processing begins which usually involves filtering and some form of blind source separation (BSS), such as ICA, to remove noise and artifact sources. Dimensionality reduction can also be performed at this step.
- At this point the data is ready for feature extraction.
- Though raw EEG and LFP time series are used for some applications, other derived features such as spectral power are frequently used as well. At this point the validation set is used for model selection and hyperparameter optimization and the final model is fit.
- Finally, aggregation techniques such as ensembling can be considered to further improve performance.

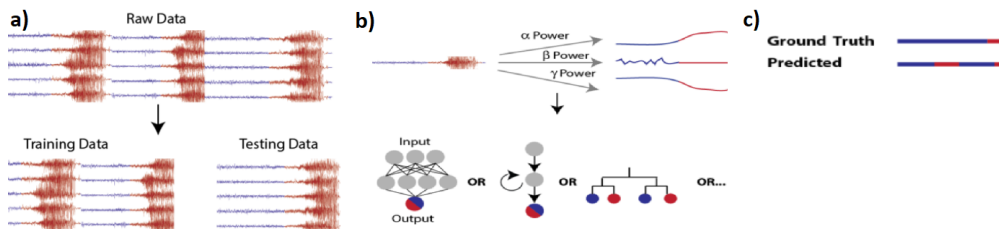


FIGURE 1.7 High-level EEG ML Pipeline: a) splitting b) feature extraction and model training c) prediction (Glaser et al., 2018).

1.6 Multielectrode Arrays & Functional Connectivity

One of the primary research interests of Neuroscience today is gaining access to characterizations of brain activity related to specific tasks, particularly in awake behaving animals. Towards this end, multi-electrode arrays spanning significant brain areas are often implanted in non-human primates. One of the earliest implementations of such a technology was published in *Cell* (Ghazanfar and Nicolelis, 1997). The largest array had sixteen electrodes and several arrays could be implanted in a single mouse. A total of 48 electrodes were implanted across several brain regions.

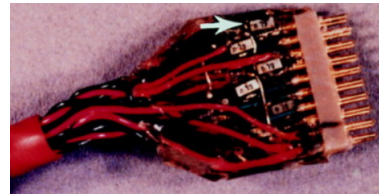


FIGURE 1.8 First multielectrode array used for *in vivo* neural data acquisition.

Now, arrays can contain upwards of a hundred electrodes and can span the entire cortex. The ability to record from hundreds of electrodes spanning across brain regions of interest is greatly informative. Unlike classic single-cell recordings, this allows recordings of the brain network across several regions and, just as importantly, the means to assess how brain connectivity between regions varies as a function of the task/load. Features such as correlation, coherence, Granger causality, and phase-slope index are often used to infer the presence and directionality of connections between regions and to characterize the networks responsible for performing particular tasks.

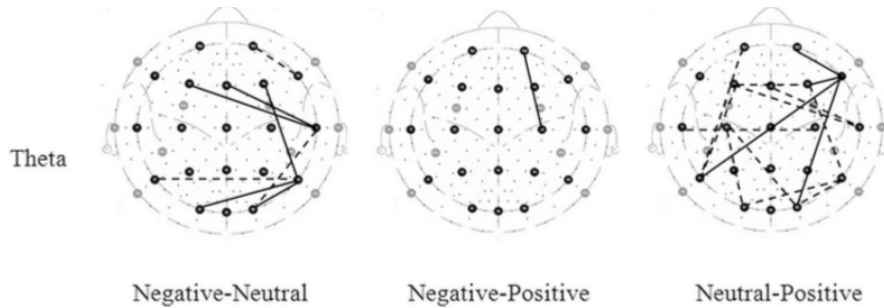


FIGURE 1.9 Discriminative support network illustrating most significant node-node interactions for emotion classification(Peng et al., 2014).

1.7 Features: Spectral Power, Covariance, and Correlation

For this specific project we used: electrode power, inter-electrode co-variance and correlation, as our three metrics of brain local activity and brain network dynamics. These three measures are meant to complement one another. Furthermore, we calculated each of these metrics within different frequency bands, as these are known to be responsible for specific brain functions. Electrode power, for example, provides insight regarding the neural activity in different spectral bands for a particular electrode. In this way, it can be considered a measure of local activity. Covariance, on the other hand, is a measure of synchronous activity between electrodes. Covariance can, therefore, be considered a measure of co-activation across brain regions. Correlation, like covariance, is also a measure of co-activation across brain regions; however, it is normalized and serves as a measure of the strength of the linear relationship between two time series. Excessive noise or a nonlinear relationship between time series will cause this measure to tend to zero. These hand-crafted features were used since they provide insight into the electrical activity in the brain. The raw

data could have been used (in conjunction with a convolutional neural network, for example) but this would have come at the cost of interpretability.

1.8 Project High-level Summary

The purpose of the project is to classify movement related neural states using iEEG and LFP data recorded from non-human primates (NHP's). The NHP's performed specific movements during a controlled experimental task, during which neural data was recorded. The data was then pre-processed and spectral power, covariance, and correlation were computed. Next, two classifiers were trained with each of the three types of metrics (power, covariance, and correlation) to identify and characterize the different mental states the NHP must assume to correctly perform the task. Finally, the discriminative support networks for each classification task were derived allowing us to visualize the most significant neural activity, both local and across regions, for movement classification.

Chapter 2

Background

The purpose of this section is to discuss the inspiration and precedent for the thesis project. As previously mentioned, EEG and LFP have been used for a myriad of classification tasks. That being said, very little has been done to classify brain states associated with the specific phases of movement preparation and production. This is what this thesis is about.

2.1 Topography of the Primary Motor Cortex

To classify brain states associated with specific movements, it is necessary to record signals emanating from neurons that are responsible for preparing and performing these actions, which for the case of multi-electrode arrays, demands the neuro-surgical implantation of intra-cortical multi-electrode arrays in several brain areas to allow for simultaneous activity recording.

Thankfully, some relevant work was performed by the Dancause Laboratory at the University of Montreal in Canada. They identified, in three adult Capuchin monkeys, the specific locations within the primary motor (M1), ventral premotor (PMv), and dorsal premotor (PMD) cortices, responsible for performing several different movements using intracortical microstimulation (ICMS). The ICSM procedure involved injecting a weak electrical current via a glass coated tungsten microelectrode into the neural tissue, while recording a grid of cortical areas to record the response (either a specific movement, or the lack thereof). If no response was observed when the current reached $100\mu A$ the point was labeled non-responsive (Dea et al., 2016). Though Figure 2.1 only shows the hand representation grid for a single animal, rep-

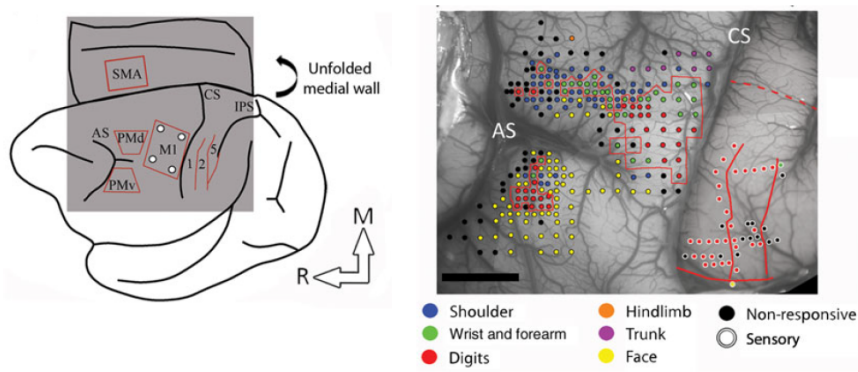


FIGURE 2.1: Brain region schematic (left) and ICMS results (right).

resentation was similar across subjects. This is key as it suggests a common neural substrate we can classify for this specific task across subjects.

The cortical surface area responsible for digit, hand, and wrist movements was also estimated for all three animals. From the bar plot, we can see a relatively large

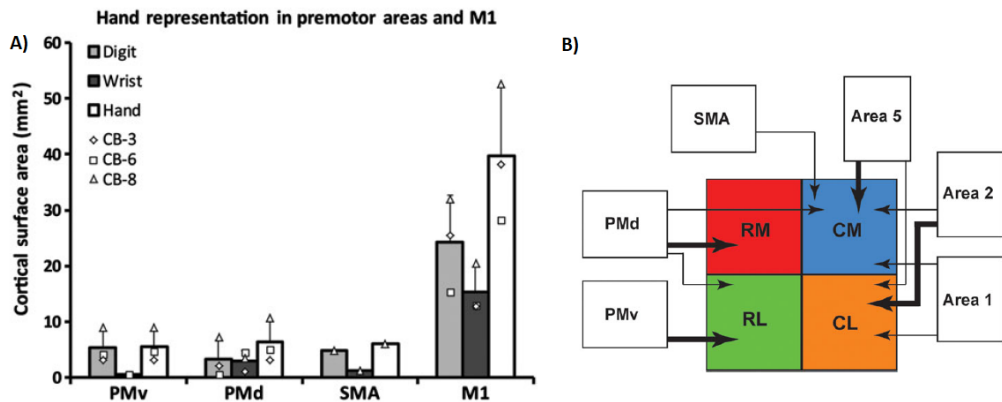


FIGURE 2.2 a) Cortical surface area responsible for performing specific movements according to brain region. b) Inter-region connections between ROI's and the M1 (split into quadrants).

portion of the M1 evoked digit, hand, and wrist movement responses. Further analyses were performed on the M1 in which the M1 was arbitrarily split in four regions labeled RM, RL, CM, and CL. Neuronal tracers were then injected in the various brain regions to measure the connectivity between areas. A visual summary of this connectivity can be seen in [Figure 2.2b](#). It is clear from the figure that the projections to the M1 are heterogeneous (as opposed to spread evenly across the M1). This is a finding that we hope to replicate via functional connectivity analyses of the recorded EEG and LFP data from these same regions.

Subsequent work by the group elucidated, to a greater extent, the high degree of modularity in the M1 region ([Hamadjida et al., 2016](#)). If this is truly the case, one might expect that recording EEG/LFP from a high density multi-electrode array from this array would provide significant insight.

2.2 Generalizability of Functional Connectivity Parameters for Classification Tasks

Pallarés ([Pallares et al., 2018](#)), along with a team of international collaborators, showed how classical functional connectivity (FC) parameters such as pairwise Pearson correlation could be expanded upon to derive subject-specific and condition-specific parameters for fMRI BOLD data. An iterative method was used to derive network effective connectivity (EC) from the classical FC correlation features. Multivariate logistic regression (MLR) and 1-nearest neighbor classifiers were used to classify subjects as well as behavioral conditions (resting state or movie watching). Both classifiers boasted impressive accuracies though the EC features yielded better results than the classical FC features. Accuracy remained high even at 30 subjects suggesting a high degree of generalization across subjects.

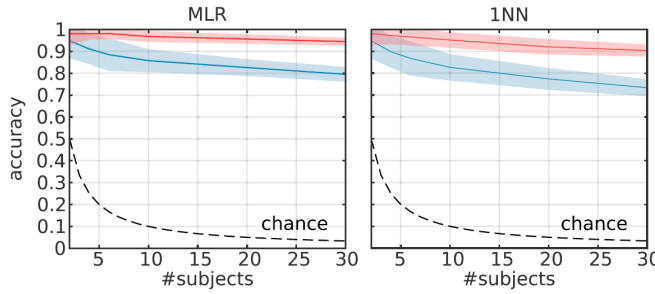


FIGURE 2.3 MLR and 1NN classifier performance using EC (red) and classical FC (blue) features.

Subsequently, recursive feature elimination (RFE) was used to extract the discriminative support network. The MLR classifier was used to perform RFE. This technique enabled the group to determine the most important nodes for classification and to produce a network associated with each classification task. The gener-

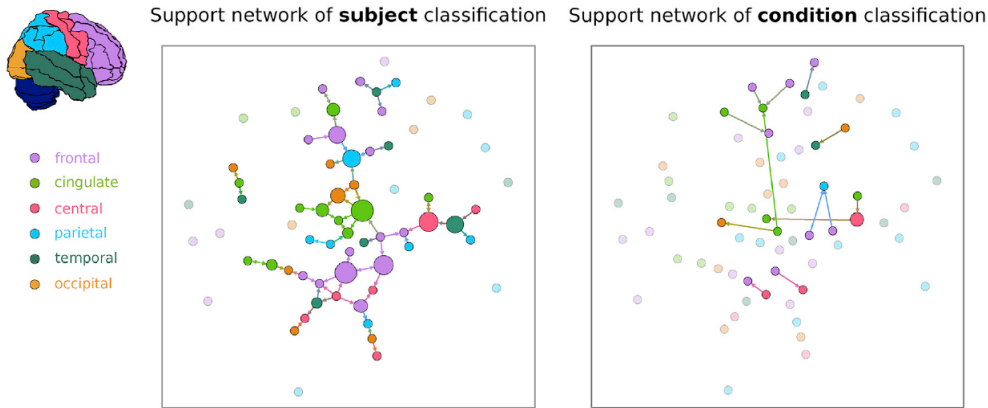


FIGURE 2.4 An electron (artist's impression).

ation of this network is especially intriguing for our study, since we already have knowledge regarding the anatomical connections between our regions of interest (ROI's). It would be excellent to reproduce the previous anatomical findings using EEG/LFP data (as opposed to ICMS and neuronal tracing as performed by Dancause, et. al.).

2.3 Classification of Movement-Related Brain States

Very little has been done to classify movement related brain states. The little that has been done has been targeted towards brain computer interfaces (BCI's). One such study was performed by Jeong Hyun Cho and his team at Korea University. The group attempted to classify hand motor execution (ME) and motor imagery (MI) from EEG data. Both the ME classification and the MI classification tasks consisted of five different hand motions and linear discriminant analysis was used for classification. The average classification accuracies for ME and MI were 56.83% and 51.01% respectively (Cho et al., 2018). Another group at Korea University performed a similar classification task involving ME and MI prediction. The group designed a hierarchical flow CNN (HF-CNN) to classify forearm movement according to three

different forearm orientations ($0^\circ, 90^\circ, 180^\circ$) using EEG(Jeong et al., 2020). The HF-

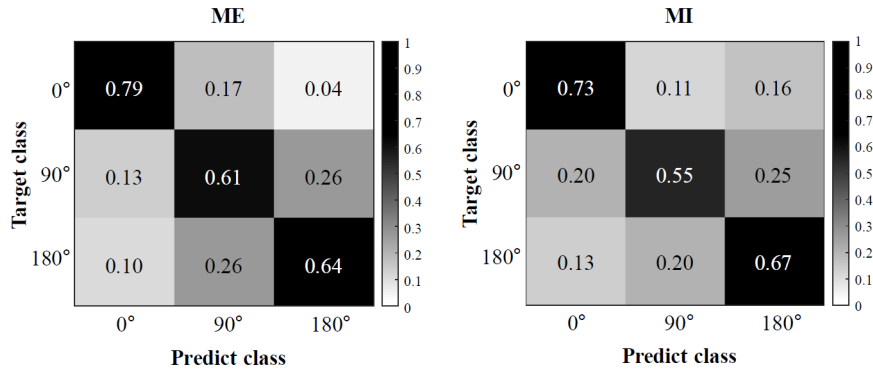


FIGURE 2.5 Confusion matrices representing HF-CNN accuracy for ME and MI tasks.

CNN boasted a grand-average classification accuracy of 0.73 for the ME task and 0.65 for the MI task. The experimental setup involved 32 surface electrodes and the EEG was sampled at 100 Hz. Three second segments of each action were used for classification and there were 50 trials for each forearm orientation.

2.4 Movement Intention Classification

A group of researchers in Japan sought to determine whether EEG signals occurring prior to movement execution could be used to classify movement intention(Kim, Yoshimura, and Koike, 2019). Recordings were collected from human subjects while performing an experiment in which they were required to move a cursor to one of two regions on a monitor They were instructed to wait for a cue before executing the movement of the cursor to the specified region. The pre-movement EEG was aggregated and split into independent components via ICA. A support vector machine classifier was fit to the components and achieved a classification accuracy of 75% in the binary classification task. This finding is pertinent since we split each experimental trial temporally into five sections of which only two include movement. Two of the remaining sections occurred pre-movement. The finding by Kim et. al. suggested it may be possible to classify these states using EEG data.

2.5 Unique Characteristics of the Present Project

The present project differs from the aforementioned studies in several key ways. Firstly, ME classification using high density LFP data is, to the best of my knowledge, unprecedented. LFP data has several advantages. The high density of the implanted electrodes, for example, should enable us to elucidate the complex interactions within small areas within brain areas. Such analysis would not be possible with mere surface electrodes. Secondly, the present project goes beyond ME classification. In fact, for this project, establishing the inter-region activity responsible for specific movements is just as important as the classification accuracy itself. Our collaborators at the University of Montreal have already established inter-region connections via neural tracer injection. We, therefore, have a ground truth model of the

connectivity which we hope to reproduce using purely LFP data. Lastly, the current data-sets consist of neural data recorded at 4096 Hz. This enabled analysis of much higher frequency ranges (the previous works involved analyses of EEG below 100 Hz). Lastly, the previous works involving ME classification were performed on healthy subjects. In our analyses, however, recordings were collected from subjects before and after the infarction induction in the M1 brain region.

Chapter 3

Methods

I will begin by explaining the two experiments performed at the Dancause Laboratory of the University of Montreal. The analysis pipeline was first developed for the dataset from Experiment 1 and preliminary analyses were performed. However, we switched to a complementary dataset (Experiment 2) since the electrode location data was required to accurately map the recorded neural signals to the specific brain regions from which they were derived. Both experiments will be discussed in this chapter, followed by a description of the machine learning methods and analysis pipeline.

3.1 Experiment 1: Reaching under Muscimol Inactivation

The goal of the experiment for the NHP was to grab and eat a pellet. The subjects started with their hands at rest in a specified location from which they would reach aiming for a target location when given the GO cue. Neural and behavioural data was recorded under two specific conditions, specifically before and after injecting Muscimol (a GABA agonist), to the left M1 brain area. This should impair digit, wrist, and forelimb movements in the right hand. Monkeys performed the pellet retrieval tasks with both hands and 256 channel EEG data was recorded during the experimental sessions.

3.1.1 Behavioral Task

In daily experimental sessions, two macaques were sat in a custom-made primate chair situated in front of an apparatus designed for pellet retrieval tasks (Figure ??). The custom chair was equipped with removable panels that allowed for restriction or allowance of movement for either arm. Some blocks of trials only allowed for movement of a single arm while others allowed for a mix. The pellet rewards were delivered in a well positioned about 10 cm below shoulder height and 20 cm from the monkeys. To get rewards, the animals were required to reach with either the left or the right arm in order to grasp a precision grip (opposition of the thumb and index fingers) with the forearm pronated. The task was controlled by a TDT acquisition system using two RZ2 BoiAmp processors and custom software ¹.

Trials

A typical trial began when the animal placed the designated hand in the home plate. Trial progression can be seen in Figure 3.1a (bottom panel). The home plate contained an infrared sensor to detect the presence of the hand and signal the start of

¹Tucker-Davis Technologies (TDT), Alachua, FL, USA

the trial. After a variable delay period between 800 and 2000ms, a pellet was delivered into the well. The clicking sound of the pellet distributor served as the GO cue for this task. The animal then initiated a self-paced reach towards the target which was also equipped with an infrared sensor to detect the presence of fingers in the slot containing the well. The animal then grasps the pellet and brings it back to their mouth to eat it. Finally, the animal places its hand back on the home plate to initiate the next trial. The inter-trial interval was 3s. Each trial was split into sections, called epochs, that were verified offline using webcam video recordings. This was necessary to confirm trial event timings and to correct for behavioral anomalies such as multiple grasps in a single trial. In each experiment session, the monkeys would perform 25 trials with each arm. Experimental sessions were performed pre and post-inactivation (see Intervention).

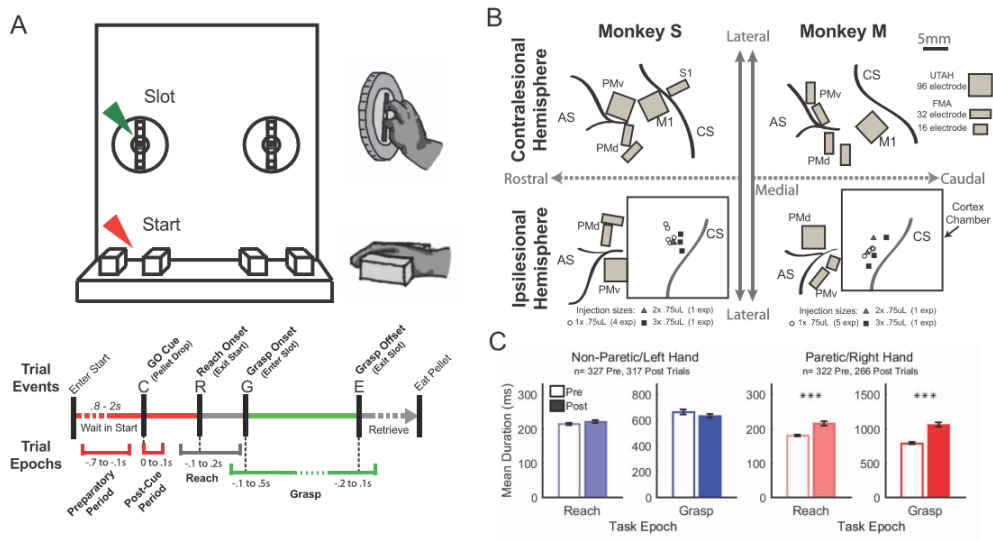


FIGURE 3.1 a) Experimental apparatus for pellet retrieval task and trial timeline. b) Multielectrode array implant schematics. c) Reach and grasp movement durations pre and post-inactivation.

3.1.2 Intervention

Monkeys were surgically outfitted with a chamber giving access to the dura for Muscimol injection. In the first two sessions, the location of the hand representation in the left M1 was confirmed via ICMS. The hand representation in the left M1 was defined as the region that, upon receiving stimulation, evoked motor responses in the digits, wrist, or arm. This area was then used to guide the Muscimol injections such that the inactivation would be contained within the M1 hand representation. The trials that took place prior to Muscimol injection are referred to as pre-inactivation trials. Subsequently, the subjects are injected with Muscimol, a GABA agonist, to inactivate the M1 hand representation area controlling movement in the right hand, wrist, and forelimb. These trials are referred to as post-inactivation trials. The intervention was effective in producing paresis (partial paralysis) in the right hand as evidenced by the increased reach and grasp times visualized in **Figure 3.1C**). The paresis in the right hand peaked in severity around the 2hr mark at which point the monkeys could not successfully perform trials. By the 10hr mark, however, the

monkeys began to regain the ability to perform the pellet retrieval task proving the transitory nature of the Musimol inactivation.

3.1.3 Neural Recordings

The present neuronal analyses are restricted to a single pre-inactivation session and the first post-inactivation session (25 minutes post-injection). This session was selected since monkeys exhibited clear deficits while still being able to perform the task for some trials. Neuronal data was recorded simultaneously from 256 channels at 4882.81Hz. The signal was then band-pass filtered between 300 and 2000Hz and recorded digitally. Neural recordings were collected from a combination of 16, 32, and 96 channel arrays (eight total). Arrays were implanted in the ventral premotor (PMv) and dorsal premotor (PMd) areas of both hemispheres as well as in the primary motor cortex of the left, contralateral, hemisphere.

3.2 Experiment 2: Reaching pre- and post-Stroke

3.2.1 High-level Summary

Two macaque monkeys were implanted with Utah electrode arrays, allowing for 256 channel LFP recordings distributed across the M1, PMv, and PMd areas. The monkeys then performed a behavioral task in which they had to reach for and grasp one of four grips on the experimental apparatus using a designated hand. The hand to be used and the grip to be grasped were communicated via light cues. If the monkey gripped the correct grip with the correct hand, a juice reward was delivered. Focused infarcts were then introduced to the portion of the left M1 area affecting the motor skills in the digits, wrist, and hand. The behavioral task was then repeated.

3.2.2 Behavioral Task

Monkeys (macaques) began by placing their hands on the home plate of the experimental apparatus. Presence of the hand was monitored via infrared sensors. After a variable resting time, two light cues would indicate which hand to use and which type of grip to reach for (either Precision or Power, four grips total). Each grip type required a different orientation of the arm and coordination of the hand to activate. Grasping the grips required pronation of the forearm. The angle of required forearm pronation could be manipulated by adjusting the grip orientation ($0^\circ, 45^\circ, 90^\circ, 135^\circ$). The GO signal in this case, was the moment the light indicators turned off. Upon turning off, the animals were allowed to grip the handles and obtain a drop of juice. There were a total of 64 recorded sessions (32 pre-stroke and 32 post-stroke). Trial progression was nearly identical to Experiment 1.

3.2.3 Intervention

Unlike the intervention performed in Experiment 1, this experiment involved inflicting physical damage to the left M1 area (as opposed to mere inactivation). To achieve this, a potent vasoconstrictive agent, endothelin-1, was administered to the left M1 in a series of 60 1 L injections occurring between 2 and 8mm below the surface of the cortex. Similar to Experiment 1, ICMS was used to determine the ROI upon which to inflict damage. The vasoconstrictive agent produced infarcts in the ROI that would take substantial time to heal.

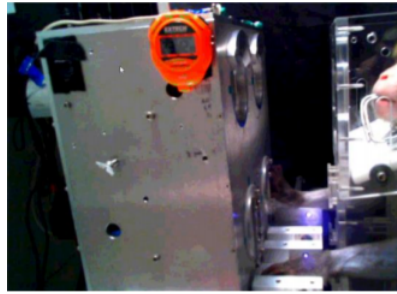


FIGURE 3.2: Macaque, in experimental apparatus, between trials.

3.2.4 Neural Recordings

Chronic high-dimensional Utah electrode arrays were implanted in the M1 of the left hemisphere as well as in the PMv and PMd of both hemispheres (five arrays total). Each array contained 96 electrodes. 256-channel LFP was sampled at 4882.81Hz and band-pass filtered between 300 and 2000Hz before being recorded digitally.

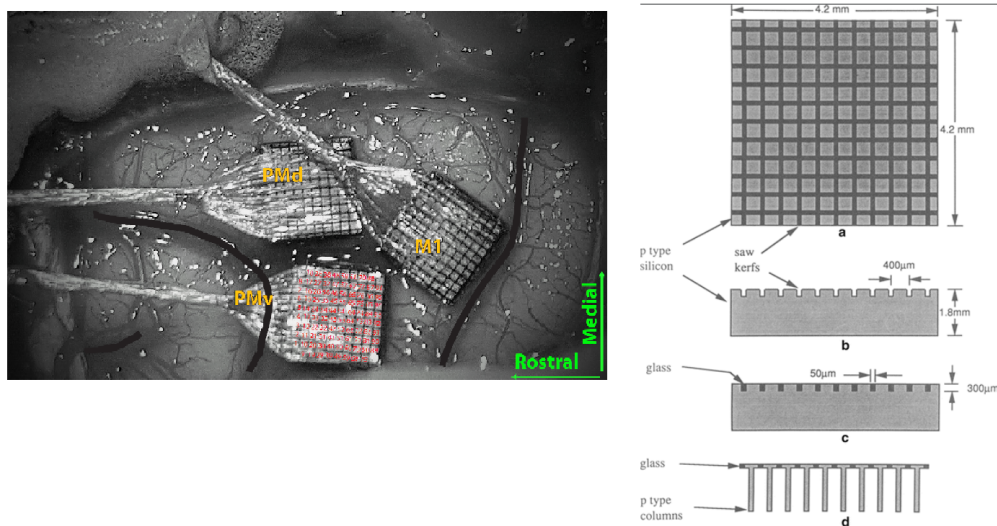


FIGURE 3.3: Three 96-electrode arrays implanted in the left hemisphere (left) and schematic of the electrode array (right).

3.3 Additional Recorded Data

Other data was recorded in addition to the neural data. Applied force to each of the handles was recorded in addition to 16 channels of electromyography² data. The EMG electrodes were implanted in the hand and forearm and. All trials were video taped as previously mentioned. Lastly, various action start times were recorded using infrared sensors.

²Time series voltage data collected from electrodes implanted in the muscle to measure muscle activity.

3.4 Analysis

3.4.1 Pre-Processing

The first several pre-processing steps were performed in MATLAB. This was done since the Dancause laboratory had it's own pre-processing pipeline using the, MATLAB-based, Brainstorm³ application. Using MATLAB enabled us to more easily mimic their pre-processing workflow. Python was then used to perform feature extraction and classification.

De-noising and Artifact Removal

Data was first band-pass filtered between 0.5 and 500 Hz to mitigate the effects of both low and high frequency electrical noise. A notch filter was also used to remove 60 Hz (and its second and third harmonics) noise due to the Mains hum phenomenon. At this point, channels were inspected visually and removed if they were heavily contaminated by noise or artifact. The number of outliers per channel was also computed where an outlier constituted data that ventured outside 15 standard deviations about the mean. There was not a hard cutoff value for inclusion but the number of outliers was heavily considered when deciding whether to keep or remove channels. Each channel was then scaled (made to have zero mean with unit variance). ICA was then performed on each connector. A single connector corresponded to 32 channels. The independent components (IC's) were visually inspected and IC's corresponding to noise or physiological artifacts (e.g. blinking) were removed. If needed, a second round of visual inspection was performed and bad segments and channels were flagged for exclusion from further analyses. Using the computed IC's, data was then divided into segments of four second duration, each representing a trial. The segments were aligned to the grasp start time which was detected by infrared sensor (time zero corresponded to the grasp start time).

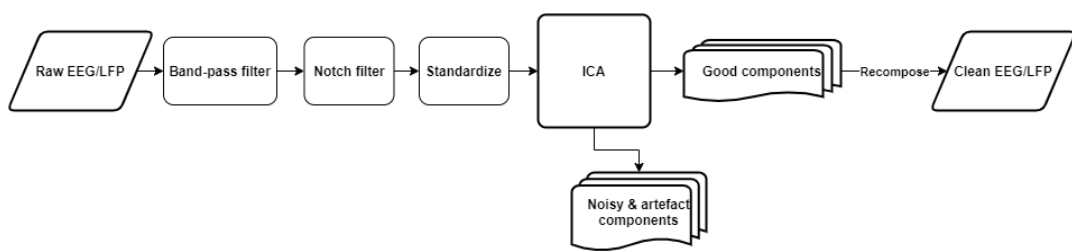


FIGURE 3.4: Neural data cleaning pipeline.

Epoching & Aggregation

Each four second trial consisted of five distinct periods: waiting for the lights indicating trial start and designated hand to illuminate, waiting for the lights to turn off (GO cue indicating the animal could begin reaching for the target), reaching for the target, grasping the Precision grip, and post-grasp. A sample of variable duration was extracted from the middle of each of these five periods. The extracted sample was generally between 0.15 and 0.25 seconds (Note: sampling frequency = 2048 Hz). The sample duration was selected as the maximum duration that allowed for

³<https://neuroimage.usc.edu/brainstorm/>



FIGURE 3.5: Trial separation schematic.

equal sampling from all trials for all actions. The number of trials was also variable since trials containing too many outliers were removed. The number of trials was between 20 and 35 for each session. Trials were categorized based on handedness (left or right) and grip orientation (0, 45, 90, or 135°).

Feature Extraction

Electrode power, correlation, and covariance were the features of choice to be extracted from the time series. Spectral power was computed for nine bandwidths: theta, alpha, beta, low gamma, gamma, low ripple, high ripple, low multi-unit, and high multi-unit. Spectral power was estimated by taking the mean of the absolute

Band Range (Hz)	Theta	Alpha	Beta	Low Gamma	High Gamma	Low Ripple	High Ripple	Low Multi-Unit	High Multi-Unit
[4,7]	[8,15]	[15,30]	[30,70]	[70,100]	[100,150]	[150,200]	[200,500]	[500,1000]	

FIGURE 3.6 Frequency ranges of the nine analyzed spectral bands.

value of each time series after applying a band-pass filter for the band of interest. This resulted in one feature for each of the N channels. Functional connectivity was calculated two ways: using sample covariance, and using Pearson correlation (Figure 3.7). In each case this resulted in $N \times N$ features where N was the number of channels.

$$\text{a)} \text{Cov}(x, y) = C_{xy} \equiv E[(x - \mu_x)(y - \mu_y)]$$

$$\text{b)} \rho_{xy} = \frac{C_{xy}}{\sqrt{C_{xx}C_{yy}}} = \frac{C_{xy}}{\sigma_x\sigma_y} = \frac{E[(x - \mu_x)(y - \mu_y)]}{\{E[(x - \mu_x)^2]E[(y - \mu_y)^2]\}^{1/2}}$$

FIGURE 3.7 a) Covariance equation b) Pearson correlation equation.

3.4.2 Classification

Logistic regression and 1-NN classifiers from the scikit-learn Python package⁴ were used to identify the five movement related neural states. The 1-NN algorithm utilized brute force to identify the nearest neighbor according to euclidean distance. The MLR was performed with a cross-entropy loss function with an added L2 regularization term with coefficient of 0.1. Optimization occurred via the limited-memory BFGS algorithm. An 80/20 train/test split was used along with stratified shuffle

⁴<https://scikit-learn.org/stable/index.html>

split cross-validation. Ten stratified shuffle splits were computed and the reported accuracies and ROCAUC's are averages. The Musimol experiment was analyzed first and served as a proof of concept. Two recording sessions of data from a single animal were analyzed (one pre-inactivation and the other post-inactivation). All channels were used, including EMG and force data, which made the task substantially easier. Moreover, only power features were computed. Then, the data from the stroke experiment was analyzed beginning with a pre-stroke session from a single animal. To further test the classification potential of the spectral power classification feature, the classifiers were tasked with identifying each of the five movement related neural states as well as the associated grip orientation (either 0 or 135°, ten states total). Finally, data from a pre-stroke session was combined with data from a post-stroke session from a single animal. From there, the five movement related states were classified for both the pre and post-stroke conditions (ten states total).

3.4.3 Feature Selection

Recursive feature elimination (RFE) was used to determine the most important electrodes for classification based on each of the three classification features (power, correlation, and covariance). The stereotaxic coordinates of the electrodes were not available and, thus, were estimated using a simple schema. The discriminative support networks displaying the 10 best power features and the 20 best FC (covariance and correlation) features were then output.

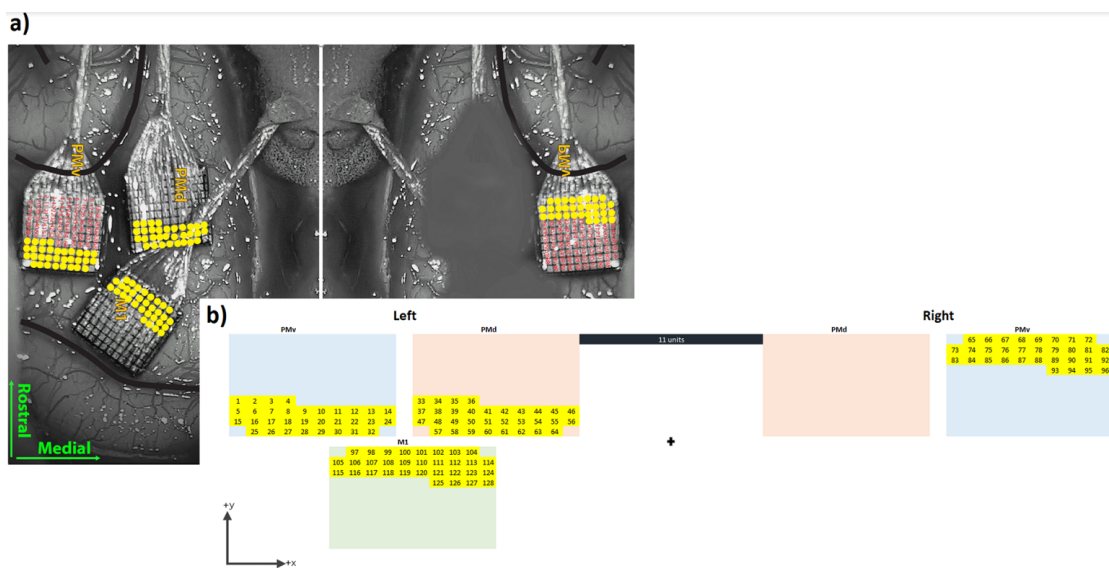


FIGURE 3.8 a) Mirrored image representing the actual layout of the arrays. Arrays excluded from the analyses were greyed out for simplicity. The yellow dots represent the electrodes included in the analyses. b) Coordinate system used to estimate the locations of the electrodes.

Chapter 4

Results

In this section, I will report the results of the analyses performed on the datasets recorded during both the Muscimol and the Stroke experiments.

4.1 Muscimol Experiment: Hand Movement Related Brain States

The first experiment involved two independent analyses of the pre- and post-inactivation sessions for a single animal, and aimed at assessing brain network differences before and after Muscimol administration in specific cortical areas. To identify those differences, two classifiers were trained on 256-channel EEG data, collected from the M1, PMv, PMd, and S1 brain areas. Only data recorded during grasping was used (0.5s sample duration). The goal of this preliminary classification was to determine which hand, left or right, was used to perform each grasp.

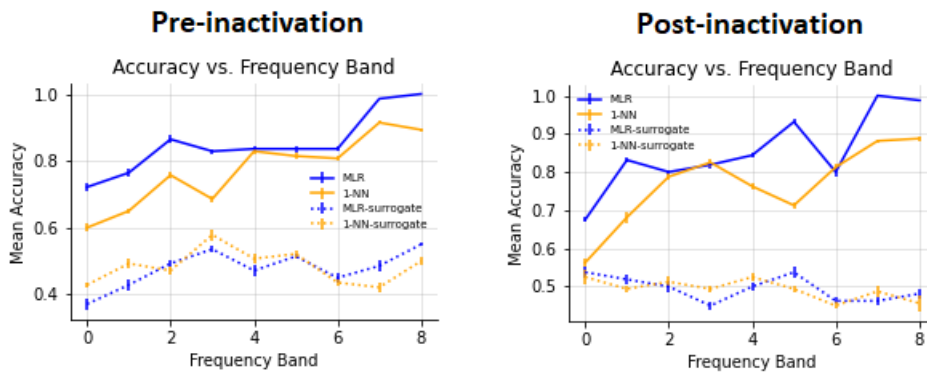


FIGURE 4.1 Pre and post-inactivation classification accuracies for each of the nine spectral bands (classification feature = spectral power).

Figure 4.5 shows that while both classifiers were able to distinguish the hand being used in each trial with high accuracy, the MLR classifier outperformed the 1-NN classifier for both the pre- and post-inactivation conditions. In fact, The MLR classifier achieved a 100% accuracy when trained on high multi-unit band power. These analyses served as an encouraging proof of concept.

4.2 Pre- and Post-stroke Action Classification

The goal of the experiment was to characterize brain activity in M1, PMv, PMd during arm reaching by means of multi-electrode simultaneous recordings and focal lesions/strokes. We split each trial into five consecutive time intervals: baseline, pre-grasp, reach, grasp, and post-grasp, to be identified from the pre- and post-stroke datasets. Typically, a single pre-intervention session preceded the stroke, and the second recording. First, the classifier was trained on band-powers from the three lowest frequency bands and performance was assessed.

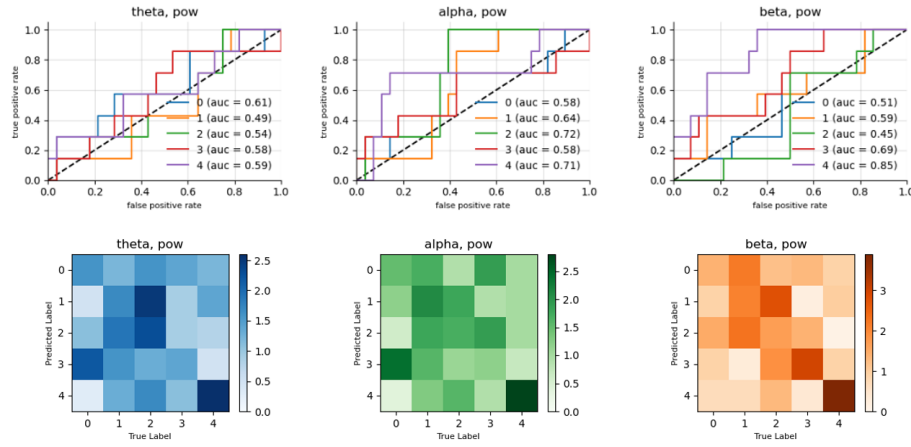


FIGURE 4.2 ROC curves and confusion matrices for the MLR classifier trained using the power in each of the three lowest frequency bands. The actions, from 0 to 4, correspond to the baseline, pre-grasp, reach, grasp, and post-grasp states.

The performance of the classifiers was poor for all five states. Interestingly, however, the classifier performed relatively well on the post-grasp state relative to the others. This can be seen visually by the relative darkness of the bottom-right-most square of the confusion matrix. It can also be seen in the magenta lines of the ROC curves and their associated AUC scores of 0.77, 0.73, and 0.87 for theta, alpha, and beta respectively. Next, the middle three frequency bands were analyzed.

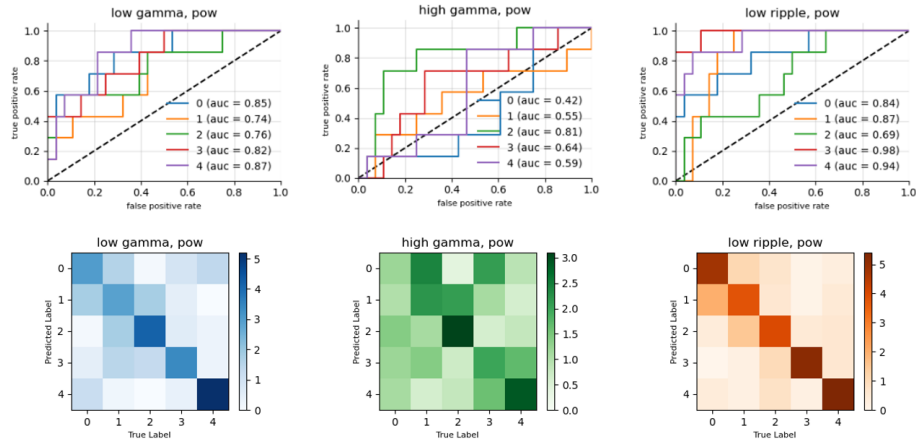


FIGURE 4.3 ROC curves and confusion matrices for the MLR classifier trained using the power in each of the three medium frequency bands. The actions, from 0 to 4, correspond to the baseline, pre-grasp, reach, and post-grasp states.

As was the case for the low frequencies, the post-grasp state was the easiest for the classifier to identify. Unlike with the low frequencies, however, the accuracies for the other four states were fairly good as well. The classifier appears to perform better using power from higher frequencies though there are some outliers (e.g. the classifier performed better with low gamma power than with high gamma power). The baseline and pre-grasp (label 0 and label 1 respectively) states appeared to be the most difficult to classify. There was a great deal of confusion between the two as seen in the confusion matrices. This is somewhat intuitive since neither of these states involved movement and the electrodes were implanted in areas of the brain that were primarily involved in motor control of the right hand. Lastly, the three highest frequency bands were analyzed.

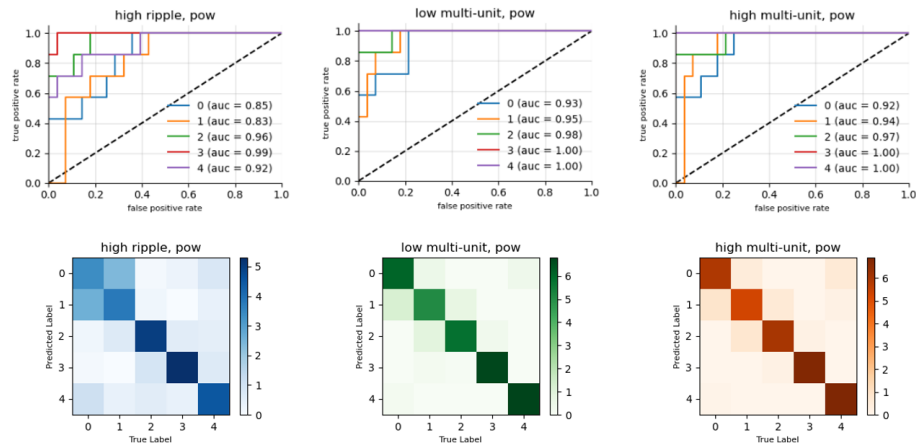


FIGURE 4.4 ROC curves and confusion matrices for the MLR classifier trained using the power in each of the three medium frequency bands. The actions, from 0 to 4, correspond to the baseline, pre-grasp, reach, and post-grasp states.

Performance continued to increase into the three highest frequency bands. An AUC score of 1 was achieved for high multi-unit power for the reach, grasp, and post-grasp states. Baseline and pre-grasp were harder to distinguish though they still achieved AUC scores of 0.92 and 0.94, respectively (for the high multi-unit frequency band). Power analyses were also performed on a post-stroke session. Similar results (see appendix) were obtained though the classifiers performed marginally worse when trained on band-power from the post-stroke session.

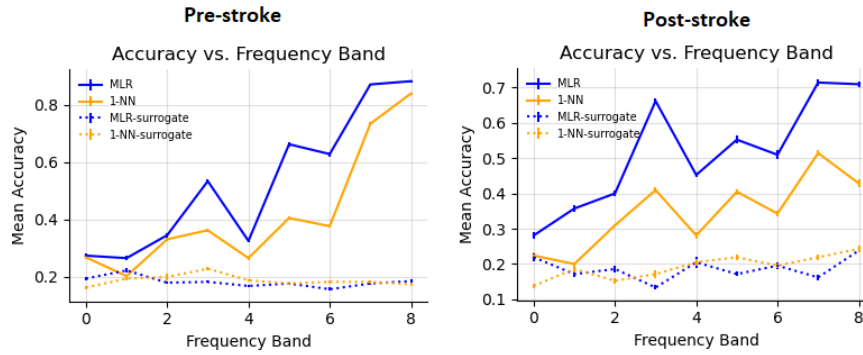


FIGURE 4.5 Pre and post-stroke classification accuracies for each of the nine spectral bands (classification feature = spectral power).

4.3 Pre-stroke Action & Orientation Classification

Inspired by the good performance in the pre-stroke session, we decided to complicate the classification task. Now, right hand trials for two different handle orientations (0° and 135°) were used. This effectively doubled the number of states. The first five states, labels 0 through 4, were extracted from the 0° pronation trials while the latter five states correspond to the 135° pronation trials.

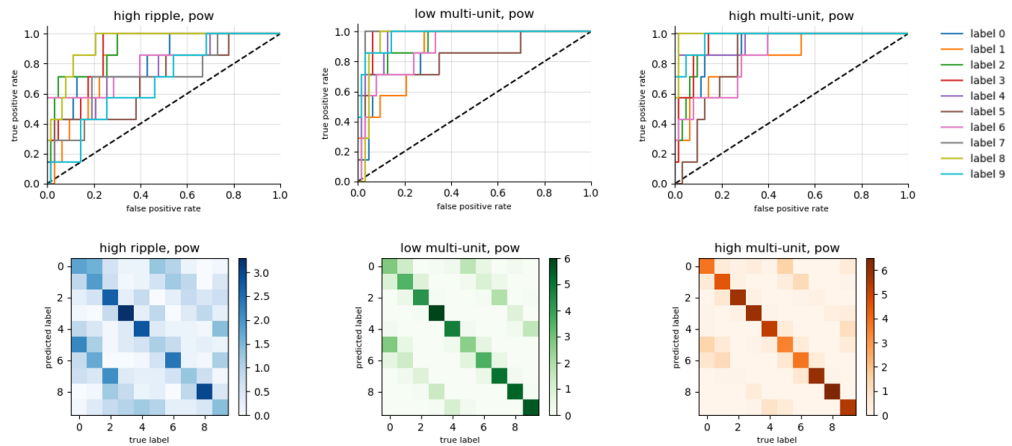


FIGURE 4.6 ROC curves and confusion matrices for the MLR classifier trained using the power in each of the three high frequency bands.

The accuracy of the classifiers followed a similar trend to the previous analyses. The classification accuracy for the three lowest frequency bands was fairly low whereas the medium frequency bands yielded better results (see appendix). The three high frequency band-powers yielded the best results; however, all accuracies were lower than the previous, single orientation analysis. This is expected due to the increase in the number of classes as well due to the remarkably similar actions the monkey was performing in the 0° and 135° conditions. During the baseline, pre-grasp, and post-grasp states, for example, one might not expect there to be much difference in the recorded brain activity since no action is being performed. Despite this, the power in the high frequencies still yielded excellent results. Though the classifier performed well, it is clear from the confusion matrices that there was some confusion between the 0° and 135° states.

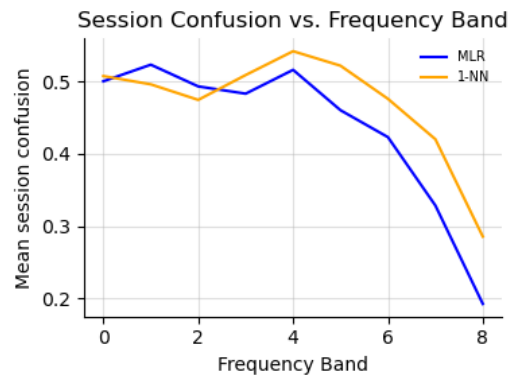


FIGURE 4.7 Session confusion plotted per frequency band (from lowest frequency to highest).

The session confusion represents the proportion of trials that were misclassified with respect to orientation. From Figure 4.7, we can see that though the confusion decreased dramatically as higher frequency band-powers were used to train the classifier, the confusion was as high as 20% even for the high multi-unit band. In fact, this orientation confusion accounted for almost all of the misclassifications.

4.4 Pre vs. Post-stroke Action Classification

For the final analysis, two sessions of LFP data were combined. LFP data from a pre-stroke session and from a session 20 minutes post-stroke were analyzed together. The first five labels represent baseline, pre-grasp, reach, grasp, and post-grasp for the pre-stroke session while the latter five labels represent the same states for the post-stroke session. As observed in the previous analyses, the low frequency band-powers yielded relatively poor results while the high frequency band-powers yielded much higher accuracies.

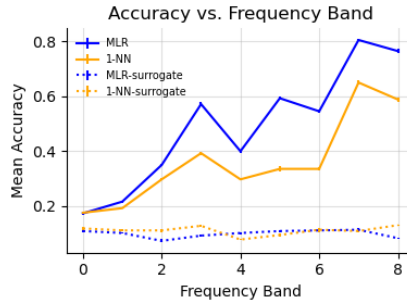


FIGURE 4.8 Accuracy plotted per frequency band (from lowest frequency to highest).

The classifier achieved higher accuracies on this task compared to the orientation classification task despite the number of classes remaining constant. This is due in large part to the lesser degree of session confusion in this task compared to the previous. In the orientation classification analysis, data from a single recording session was used. In this analysis (pre-stroke vs. post-stroke), however, data from two different recording sessions were used. This could have introduced confounds that enabled the classifier to more easily distinguish the pre and post-stroke conditions.

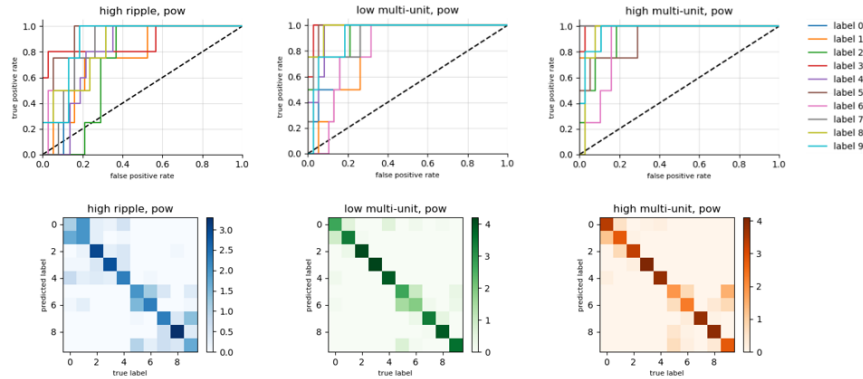


FIGURE 4.9 ROC curves and confusion matrices for the MLR classifier trained using the power in each of the three high frequency bands.

As seen in the session confusion plot, there was almost no confusion between the pre and post-stroke sessions, especially for the higher frequency bands.

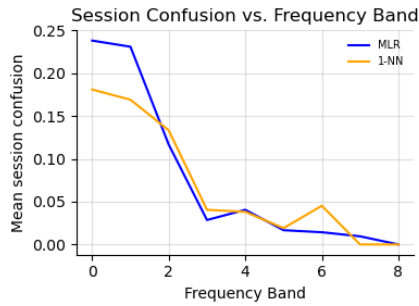


FIGURE 4.10 Session confusion plotted per frequency band (from lowest frequency to highest).

RFE was then performed to determine the ten electrodes that contributed the most to the MLR classifier's accuracy.

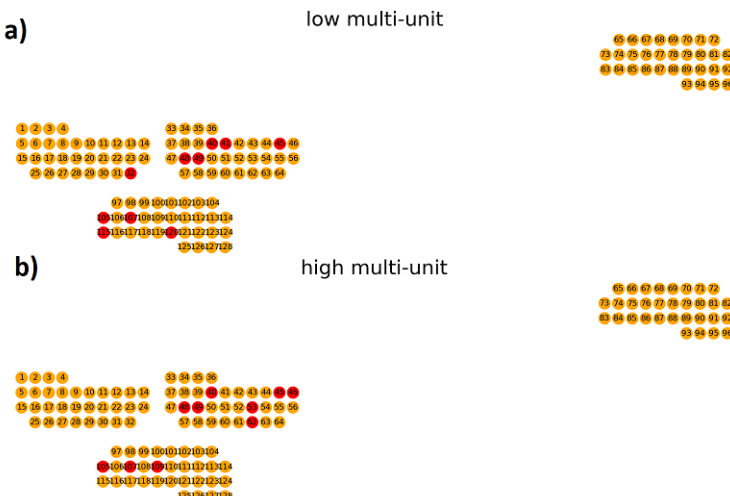


FIGURE 4.11 a) Discriminative network projection for the low multi-unit band. b) Discriminative network projection for the high multi-unit band.

These two bands were chosen since they both achieved near 80% accuracy. Interestingly, five of the ten most significant electrodes were shared between the two bands. All the significant electrodes bar one were located in the left M1 and PMd brain areas. No significant electrodes were selected from the right hemisphere for either spectral band. Functional connectivity analysis was then performed to complement the spectral band power analysis. Covariance was the next computed classification feature.

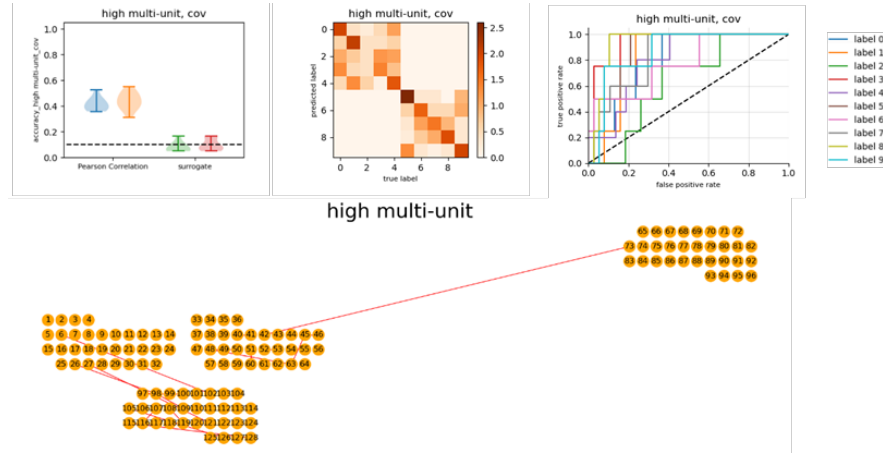


FIGURE 4.12 High multi-unit covariance analysis. From left to right: Average accuracy violin plot for MLR (blue) and 1-NN (orange) classifiers. The green and red indicate accuracy of the MLR and 1-NN when the training set labels were randomized. Confusion matrix for the MLR classifier. ROC curve for MLR classifier. Bottom: Discriminative support network projection showing the 20 most significant electrodes for classification.

In the power analyses, the reaching and grasping states tended to be classified with higher accuracy than the baseline and pre-grasp states. In stark contrast to that trend, the covariance classification feature yields the opposite result. The baseline, pre-grasp, and post-grasp states were classified with higher accuracy than the reach and grasp states. The discriminative support network, however, illustrates a similar trend to the prior power analyses in that the majority of activity occurred in the left hemisphere. Furthermore, the majority of significant connections occurred in the M1. Unlike in the power analyses, however, there was a significant electrode in the right hemisphere. Finally, correlation was analyzed.

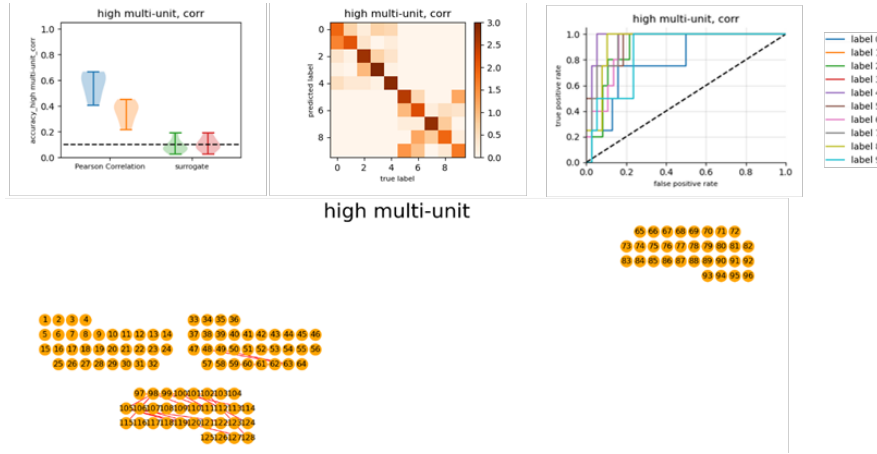


FIGURE 4.13 High multi-unit correlation analysis. From left to right:
Average accuracy violin plot for MLR (blue) and 1-NN (orange) classifiers. The green and red indicate
accuracy of the MLR and 1-NN when the training set
labels were randomized. Confusion matrix for the MLR
classifier. ROC curve for MLR classifier. Bottom:
Discriminative support network projection showing
the 20 most significant electrodes for classification.

The correlation analysis yielded higher classification accuracies than the covariance analysis. The correlation classification feature yielded results more similar to the power analysis in that the reach and grasp states were classified with the highest accuracy (as seen in the confusion matrix). Another similarity between the correlation and power analyses is the lack of significant activity involving the right hemisphere. Lastly, the majority of significant inter-electrode interaction took place within the M1 and no inter-region connections were selected.

Chapter 5

Discussion

The goal of this study was to first assess whether movement-related brain states could be identified and characterized by machine learning methods, in two LFP datasets recorded from non-human primates at the Dancause Laboratory in Montreal. Based on some preliminary results we opted to pursue further analyses on the effect that pharmacology (muscimol) and controlled strokes would exert on the brain network involved in movement production.

We separated our data by frequency band, and analysed each band's contribution to different brain states during task performance according to three metrics: electrode power, covariance between electrodes, and correlation between electrodes. Our main result shows that the machine learning classifiers and algorithms were successful in ranking a frequency-band increasing contribution to the configuration of specific brain states during particular movement phases. Loosely speaking, the higher the frequency, the better the distinction between movement-related neural states.

The power analysis we performed on the Musimol experiment dataset exemplified the potential of LFP-derived spectral power features for simple classification tasks. Both the low and high multi-unit bands achieved perfect, or near perfect accuracy. This was, however, a simple binary task. From there, we segmented trials from the stroke experiment into five distinct states: baseline, pre-grasp, reach, grasp, and post-grasp. Once again, both the low and high multi-unit band spectral power features resulted in near perfect classification with AUC scores above 0.9 for all five movement states.

In the classification task was complicated yet again in an effort to measure the predictive power of these spectral power features. To achieve this, the number of classes was doubled by introducing the pronation angle condition (either 0° or 135°). We predicted this would result in a significant downturn in classification accuracy due to the doubling in the number of classes as well as due to pronation angle only being a factor during two of the five movement states. Nevertheless, the AUC scores for all classes were above 0.8 for the low and high multi-unit band power features. In contrast Jeong et. al. achieved a grand average accuracy of 0.73 when classifying just three orientation dependent states(Jeong et al., 2020). They also used a markedly more sophisticated classifier (HF-CNN), performed more trials, and took samples of larger durations during each movement.

Finally, a pre and post-stroke session were aggregated and analyzed together. This yielded similar AUC scores to the orientation analysis, though, the confusion between the pre-stroke and post-stroke conditions was considerably less than for the two movement orientations. We then computed the functional connectivity (covariance and coherence) between the 128 implanted electrodes. These features resulted in lower classification accuracy than the spectral power features though the accuracies were considerably higher than random chance.

Lastly, we generated discriminative support networks showing the most significant electrodes according to spectral power and FC in different frequency ranges. Almost all the electrodes selected by the RFE were located in the left hemisphere which is to be expected since we used trials in which the right hand was used to perform the movement execution task. We also observed a couple of significant PMv-M1 connections which were also observed by Numa et. al. in their 2016 publication(Dea et al., 2016).

5.1 Limitations

While we did our best to equally clean each dataset, the current pipeline necessarily exhibits some limitations, which we aim at overcoming in future versions of the code. Specifically, one limitation is the required level of training when removing specific ICA components related to eye movements or other artefacts, which obliged to run the process several times for the same dataset. Furthermore, slight differences in the pre-processing for different sessions could unintentionally simplify the classification task when more than one session was involved (such as in the pre vs. post-stroke analysis). Moreover, if inconsistent pre-processing occurred, the RFE might include/remove a few non physiologically relevant electrodes. This would effectively introduce noise in the results. Another drawback was that exceedingly short samples were extracted from each of the five movement tasks. The sample duration ranged between 0.17s and 0.25s for the various analyses. As previously mentioned, the sample duration was the maximum duration allowing for equal sampling of all movement tasks for all trials. This was done to simplify the analysis and the pipeline could be altered to allow for samples of varying durations. In addition to drawbacks inherent to the pipeline, there were drawbacks inherent to the dataset as well. Stereotactic electrode coordinates, for example, were not recorded and, thus, needed to be estimated. Furthermore, the EEG and LFP data were band-pass filtered during acquisition. The lower cutoff frequency was 300Hz which resulted in attenuation of the low frequencies. This may have negatively impacted the classification accuracy in the lower frequency bands. Lastly, RFE was extremely computationally intensive and required three or four days to calculate the results for a single frequency band.

5.2 Future Work

There are many improvements that could be implemented in future works:

- Firstly, more sophisticated classification methods than MLR and 1-NN could be used. A convolutional neural network such as the one proposed by Jeong et. al. would likely increase classification accuracy(Jeong et al., 2020). It would, however, come at the cost of decreased interpretability unless significant algorithmic alterations were made.
- Covariance and correlation of the EEG and LFP time series were only computed for lag zero. A multitude of lags could be explored though the resulting feature matrix would be colossal, thus, necessitating a less computational intensive feature selection method than RFE.
- Effective connectivity, as opposed to classical as outlined by Pallares et. al. could result a higher degree of separability of the classes (Pallares et al., 2018).

Furthermore, effective connectivity is inherently directional which would provide additional insight.

- Sessions from several subjects could be analyzed to test whether the classifiers could generalize across subjects.
- Finally, group-level component pre-processing could be explored which would prevent the possibility of introducing bias via inconsistent pre-processing between sessions(Huster, Plis, and Calhoun, 2015).

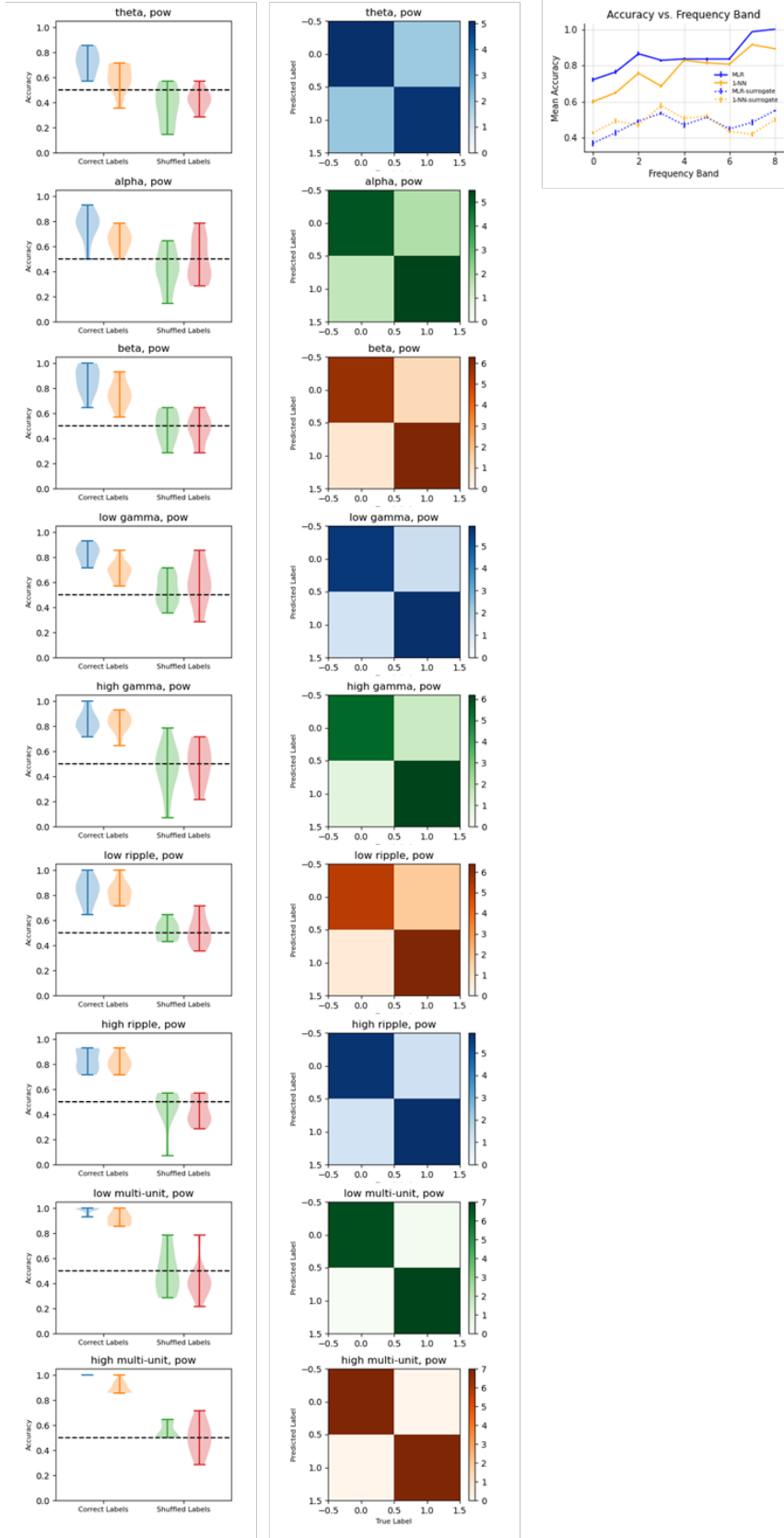
5.3 Conclusions

The provided high density and high sampling rate LFP dataset proved to posses great predictive power. We showed that this relatively untapped neural data modality could be used to classify movement execution and orientation, pathological states (stroke or inactivation), and even movement intention with high accuracy despite a relatively large number of classes. Furthermore, this level of performance was achieved despite small sample durations, few trials, and the use of a relatively unsophisticated classifier (at least compared to deep neural networks). There are many ways to improve and expand upon the current work and it will be exciting to see what the future holds for this data modality.

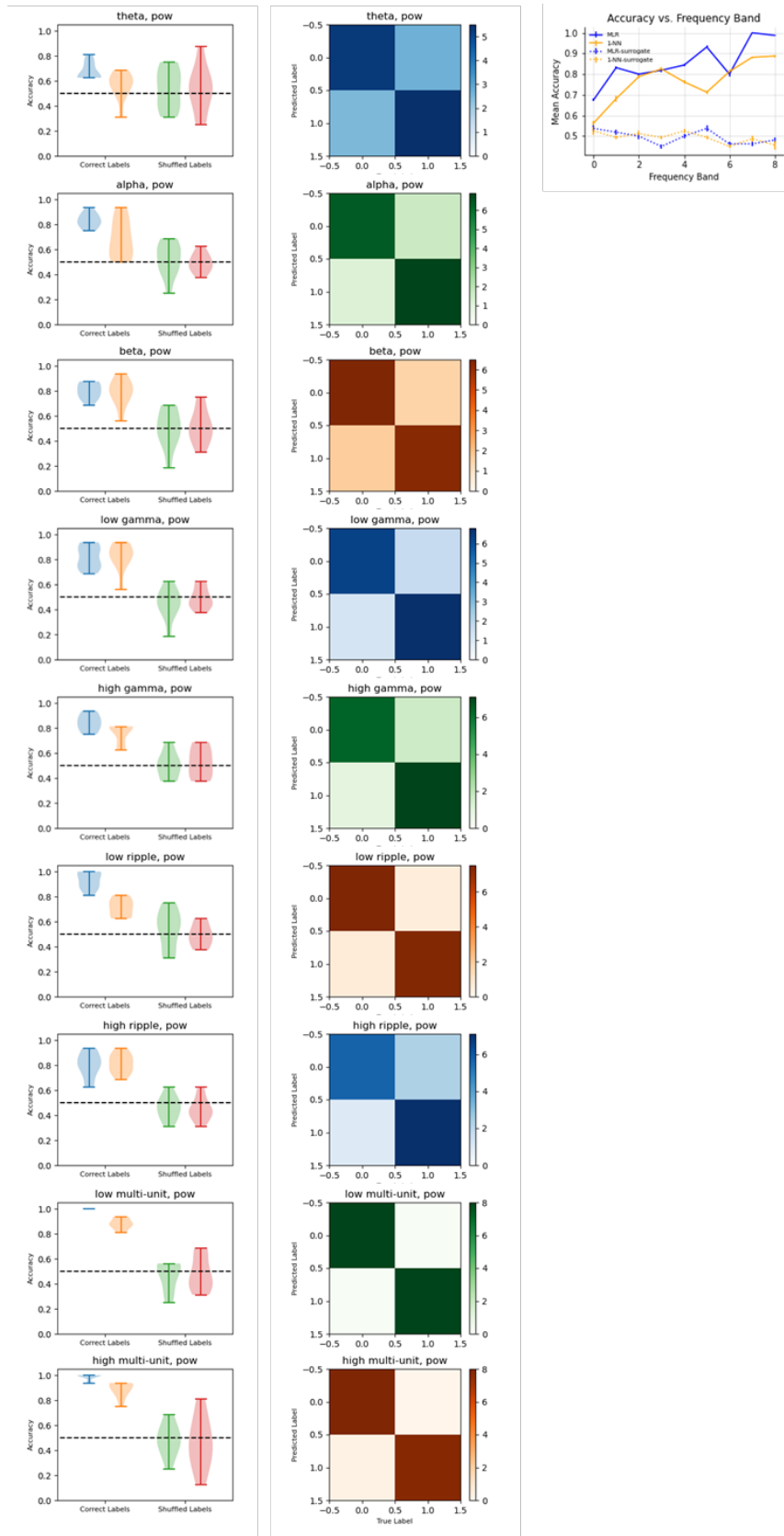
Appendix A

Power Analysis

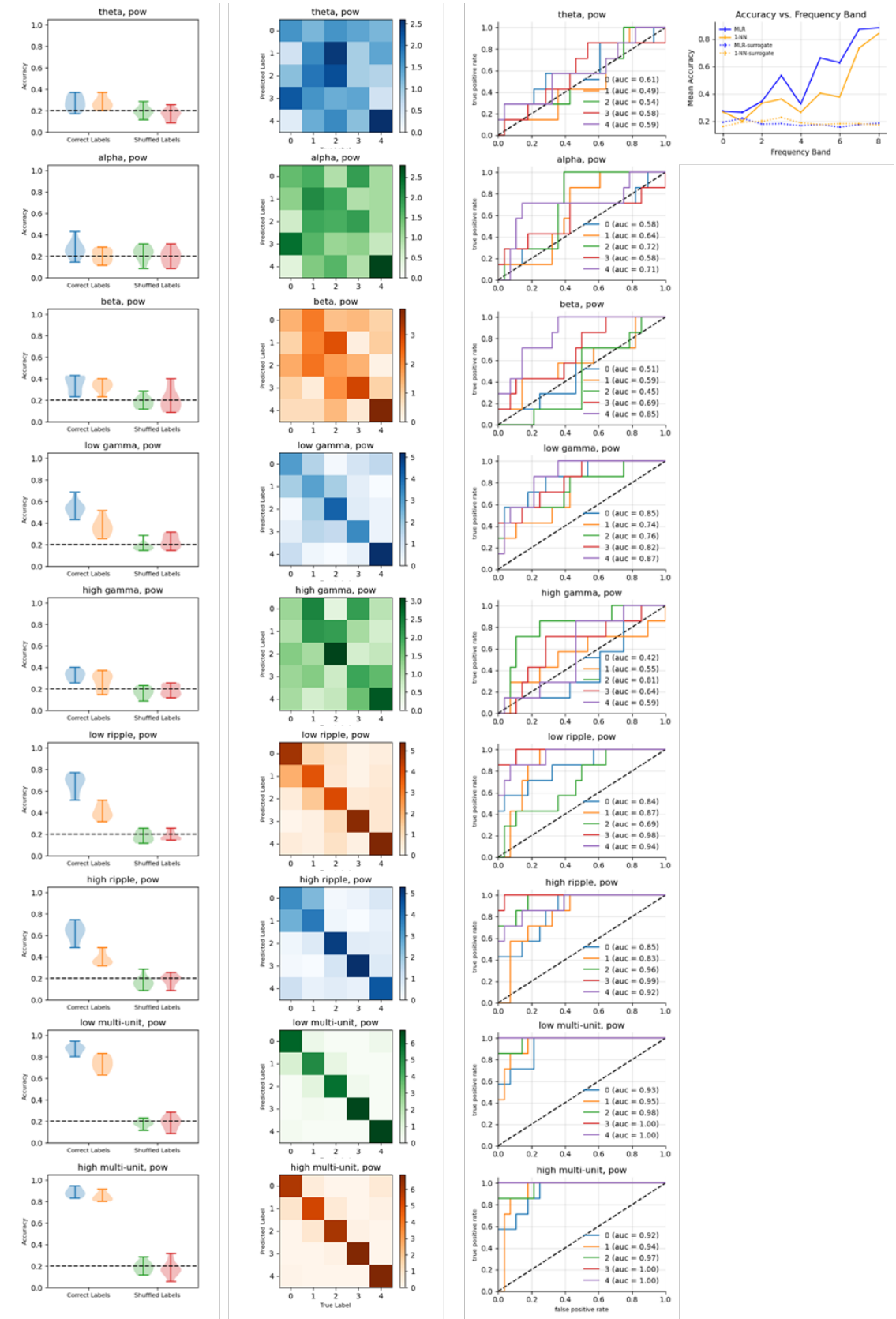
A.1 Pre-Muscimol Inactivation Power Analysis



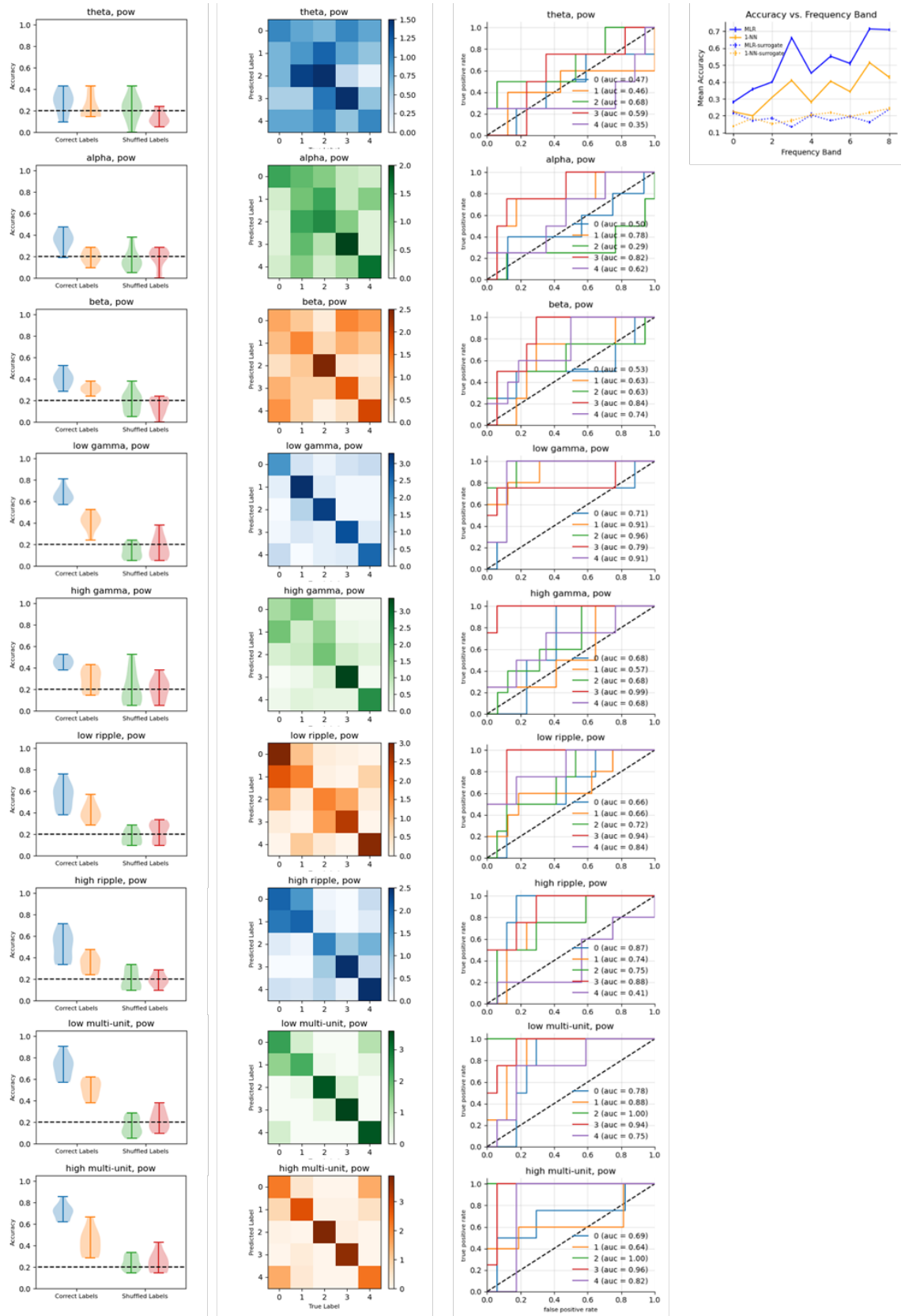
Post-Muscimol Inactivation Power Analysis



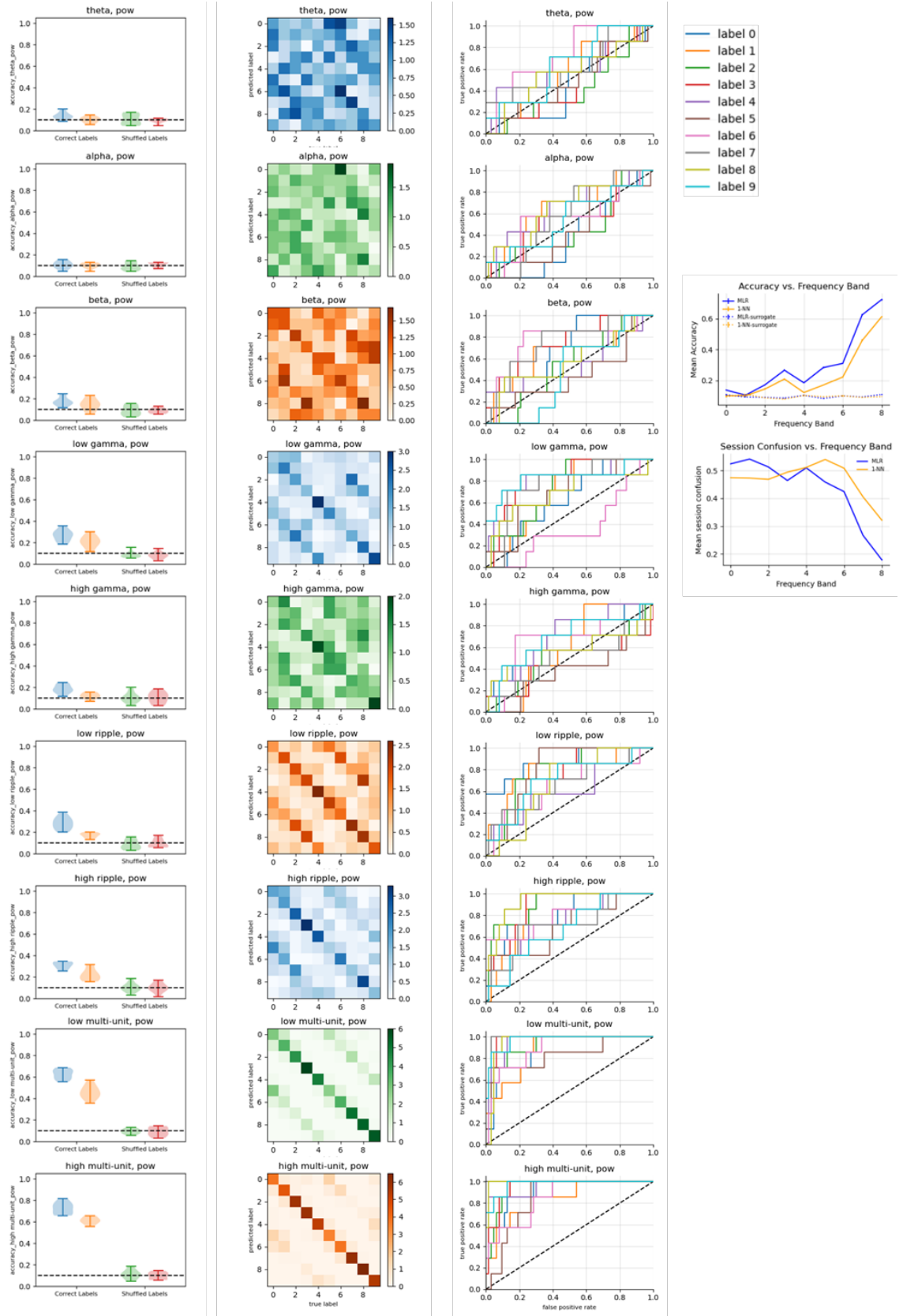
Pre-stroke Power Analysis



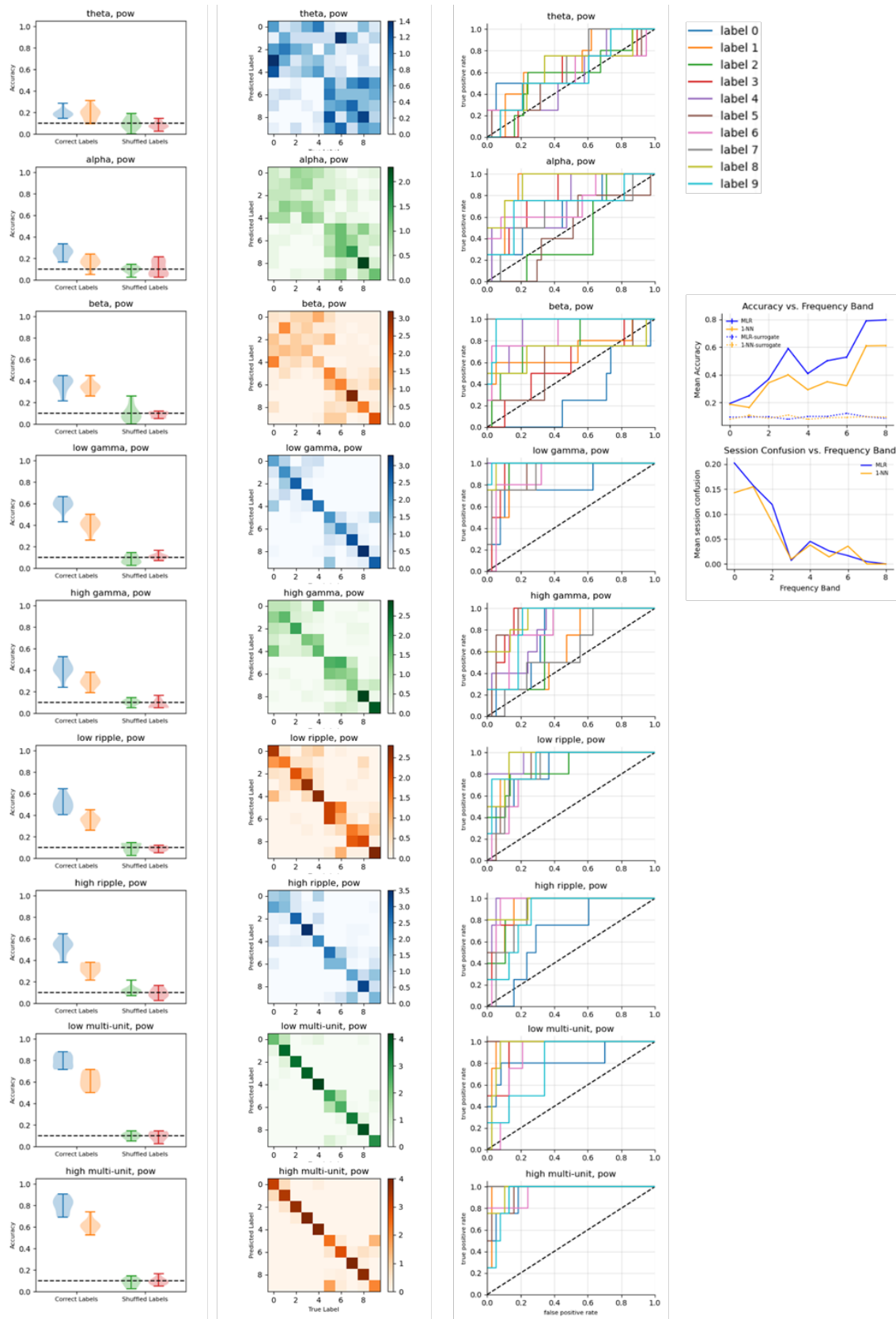
Post-stroke Power Analysis



Pre-stroke Orientation Power Analysis



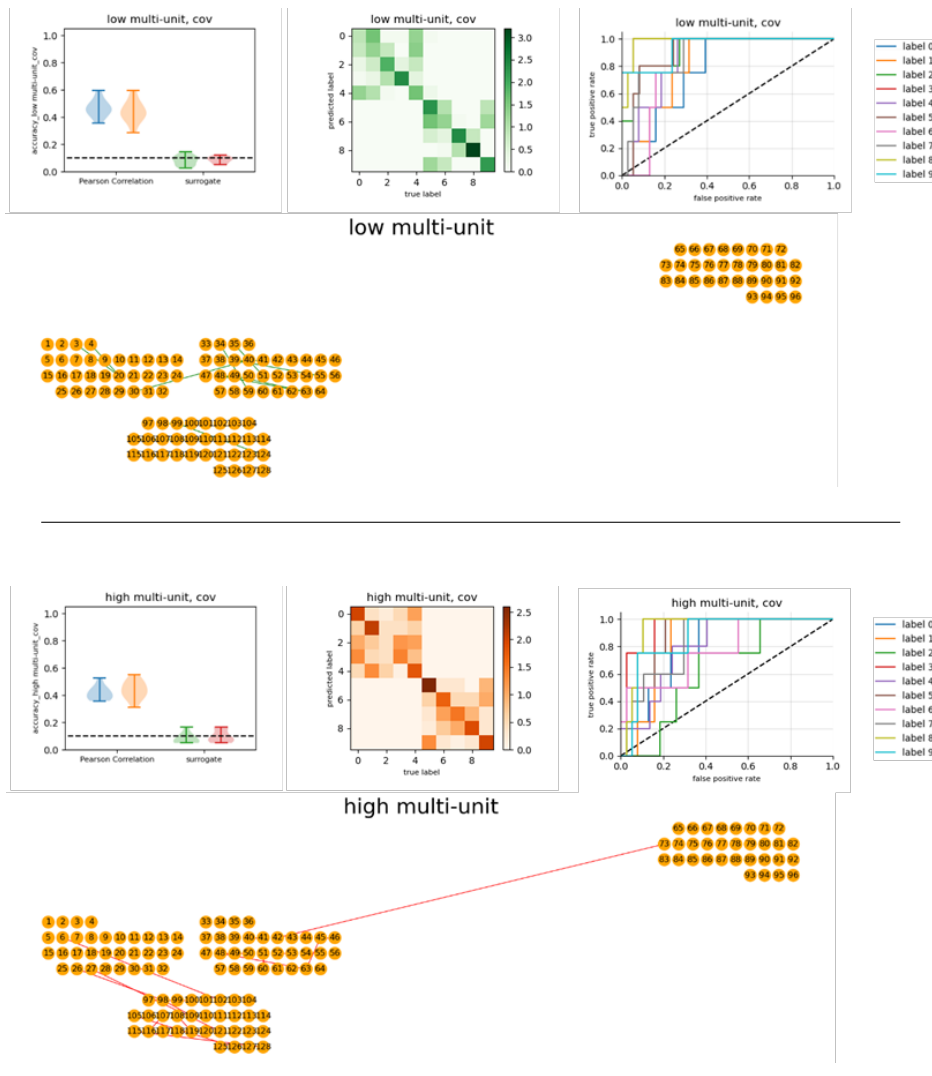
Pre-stroke vs. Post-stroke Power Analysis



Appendix B

Covariance Analysis

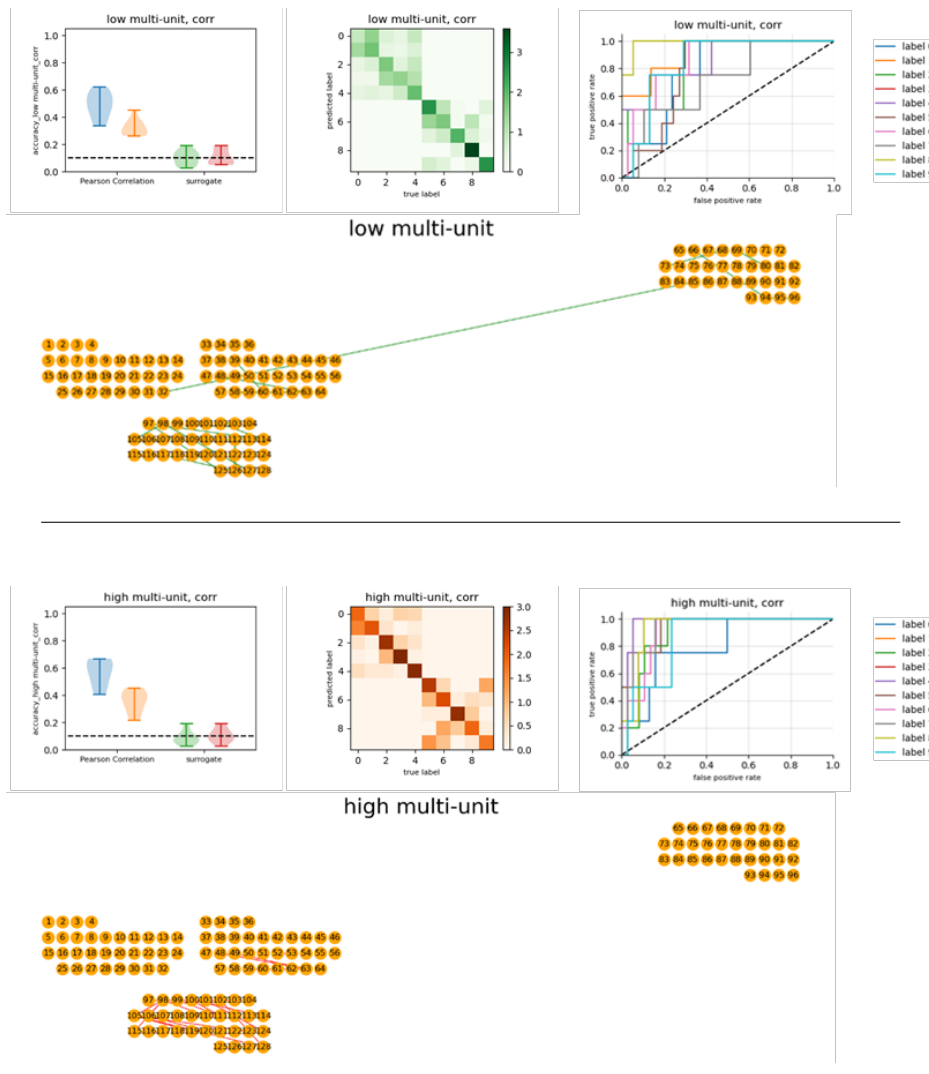
B.1 Pre vs. Post-stroke Covariance Analysis



Appendix C

Correlation Analysis

C.1 Pre vs. Post-stroke Correlation Analysis



Bibliography

- Caton, Richard and B.S. Schoenberg (1974). "Richard Caton and the electrical activity of the brain". In: *Mayo Clin. Proc.* 49.7, pp. 474–481.
- Cho, J. et al. (2018). "Classification of Hand Motions within EEG Signals for Non-Invasive BCI-Based Robot Hand Control". In: *2018 IEEE International Conference on Systems, Man, and Cybernetics (SMC)*, pp. 515–518.
- Craik, Alexander, Yongtian He, and Jose L Contreras-Vidal (2019). "Deep learning for electroencephalogram (EEG) classification tasks: a review". In: *Journal of Neural Engineering* 16.3, p. 031001. DOI: [10.1088/1741-2552/ab0ab5](https://doi.org/10.1088/1741-2552/ab0ab5). URL: <https://doi.org/10.1088/1741-2552/ab0ab5>.
- Dea, Melvin et al. (2016). "Different Patterns of Cortical Inputs to Subregions of the Primary Motor Cortex Hand Representation in *Cebus apella*". In: *Cereb. Cortex* 26.4, pp. 1747–1761.
- Ghazanfar, Asif and Miguel Nicolelis (1997). "Nonlinear processing of tactile information in the thalamocortical loop". In: *J. Neurophysiol.* 78.1, pp. 506–510.
- Glaser, Joshua I. et al. (2018). *The Roles of Supervised Machine Learning in Systems Neuroscience*. arXiv: [1805.08239 \[q-bio.NC\]](https://arxiv.org/abs/1805.08239).
- Grinvald, Amiram and Rina Hildesheim (2004). "VSDI: a new era in functional imaging of cortical dynamics". In: *Nat. Rev. Neurosci.* 5.11, pp. 874–885.
- Hamadjida, Adjia et al. (2016). "Parallel Cortical Networks Formed by Modular Organization of Primary Motor Cortex Outputs". In: *Current Biology* 26.13, pp. 1737–1743. ISSN: 0960-9822. DOI: <https://doi.org/10.1016/j.cub.2016.04.068>. URL: <http://www.sciencedirect.com/science/article/pii/S0960982216304626>.
- Huster, Rene, Sergey Plis, and Vince Calhoun (2015). "Group-level component analyses of EEG: validation and evaluation". In: *Front Neurosci* 9, p. 254.
- Jeong, J. et al. (2020). "EEG Classification of Forearm Movement Imagery Using a Hierarchical Flow Convolutional Neural Network". In: *IEEE Access* 8, pp. 66941–66950.
- Jiang, X., G. B. Bian, and Z. Tian (2019). "Removal of Artifacts from EEG Signals: A Review". In: *Sensors (Basel)* 19.5.
- Kim, Hyeonseok, Natsue Yoshimura, and Yasuharu Koike (2019). "Classification of Movement Intention Using Independent Components of Premovement EEG". In: *Frontiers in Human Neuroscience* 13, p. 63. ISSN: 1662-5161. DOI: [10.3389/fnhum.2019.00063](https://doi.org/10.3389/fnhum.2019.00063). URL: <https://doi.org/10.3389/fnhum.2019.00063>.
- Lisha Sun, Ying Liu, and P. J. Beadle (2005). "Independent component analysis of EEG signals". In: *Proceedings of 2005 IEEE International Workshop on VLSI Design and Video Technology, 2005*. Pp. 219–222.
- Macé, Émilie et al. (2018). "Whole-Brain Functional Ultrasound Imaging Reveals Brain Modules for Visuomotor Integration". In: *Neuron* 100.5, 1241–1251.e7. ISSN: 0896-6273. DOI: <https://doi.org/10.1016/j.neuron.2018.11.031>. URL: <http://www.sciencedirect.com/science/article/pii/S0896627318310407>.

- Pallares, Vicente et al. (Sept. 2018). "Extracting orthogonal subject- and condition-specific signatures from fMRI data using whole-brain effective connectivity". In: *Neuroimage* 178, pp. 238–254.
- Peng, Y. et al. (2014). "EEG-based emotion recognition with manifold regularized extreme learning machine". In: *2014 36th Annual International Conference of the IEEE Engineering in Medicine and Biology Society*, pp. 974–977.